



NACA

RESEARCH MEMORANDUM

FOR REFERENCE

EFFECT OF SECTION THICKNESS AND TRAILING-EDGE RADIUS ON ^{NOT TO BE TAKEN FROM THIS ROOM}

THE PERFORMANCE OF NACA 65-SERIES COMPRESSOR

BLADES IN CASCADE AT LOW SPEEDS

By L. Joseph Herrig, James C. Emery, and John R. Erwin

Langley Aeronautical Laboratory
Langley Field, Va.

LIBRARY

LIBRARY, NACA
LANGLEY STATION
HAMPTON, VIRGINIA

CLASSIFICATION CHANGED TO UNCLASSIFIED

AUTHORITY: NACA RESEARCH ABSTRACT NO. 98

DATE: MARCH 26, 1956

CLASSIFIED DOCUMENT

This material contains information affecting the National Defense of the United States within the meaning of the espionage laws, Title 18, U.S.C., Secs. 793 and 794, the transmission or revelation of which in any manner to an unauthorized person is prohibited by law.

NATIONAL ADVISORY COMMITTEE FOR AERONAUTICS

WASHINGTON

December 13, 1951



NATIONAL ADVISORY COMMITTEE FOR AERONAUTICS

RESEARCH MEMORANDUM

EFFECT OF SECTION THICKNESS AND TRAILING-EDGE RADIUS ON
THE PERFORMANCE OF NACA 65-SERIES COMPRESSOR
BLADES IN CASCADE AT LOW SPEEDS

By L. Joseph Herrig, James C. Emery, and John R. Erwin

SUMMARY

NACA 65-series compressor blades cambered to an isolated airfoil lift coefficient of 1.2 have been tested in a low-speed porous-wall cascade with maximum section thicknesses of 6, 8, 10, 12, and 15 percent of the chord to obtain the effect of maximum section thickness on section operating characteristics. These sections were tested over the useful angle-of-attack range at inlet angle, β , and solidity, σ , combinations of $\beta = 45^\circ$, $\sigma = 1.5$ and $\beta = 60^\circ$, $\sigma = 1.0$ and 1.5. A 10-percent-thick section tested with a trailing-edge radius of 1 and 2 percent chord was compared with data for a similar section having the usual 0.15-percent radius to determine the penalties incurred with more practical trailing edges. This section was tested at inlet angle and solidity combinations of $\beta = 45^\circ$, $\sigma = 1.5$ and $\beta = 60^\circ$, $\sigma = 1.0$.

From the results of this investigation, increasing compressor blade thickness from 6 percent to 15 percent chord appears to have no significant effect on the design angle of attack, but reduces the design turning angle from 2° to 4° , depending on the inlet angle and solidity considered. The low-speed operating range (limits taken as the angles of attack for which the drag coefficient is twice the minimum value) increases about 50 percent as the section thickness is increased from 6 percent to 15 percent chord. Sections having trailing-edge radii equal to 10 percent of the maximum section thickness are recommended for practical construction.

INTRODUCTION

The low-speed performance of NACA 65-series compressor blades in cascade is presented in reference 1 over a wide range of inlet angle, solidity, and camber for sections of 10 percent maximum thickness. Design charts are presented to permit the selection of a suitable camber



and angle of attack to produce a desired turning angle, the inlet angle of the flow and the solidity of the blades being known. In aircraft axial-flow compressors, blade sections of maximum thickness other than the average value of 10 percent are used for most of the blade length. Information is desired to indicate the changes in performance to be expected if the section maximum thickness is varied from 10 percent chord in order to apply the data and design charts of reference 1 to the actual case. Therefore, the test program of reference 1 was extended to include tests of blade sections of one camber with maximum thickness varied from 6 percent to 15 percent of the blade chord at three combinations of inlet angle and solidity. Two of the combinations selected $\beta = 45^\circ$, $\sigma = 1.5$ and $\beta = 60^\circ$, $\sigma = 1.0$ are considered to be typical of usual axial-flow compressor conditions. The third combination $\beta = 60^\circ$, $\sigma = 1.5$ was studied because the section thickness was expected to produce more pronounced effects at this high-inlet-angle, high-solidity condition, thus aiding in establishing trends.

As a further practical consideration, current mass-production blade-construction methods require greater thickness in the region near the blade trailing edge than is provided by the basic thickness shape used for the tests of reference 1. It is desirable to know the penalty, if any, which is being paid for ease of construction in order to determine if there is any need for development of improved construction methods. In view of this, the NACA 65-(12)10 blade section was tested at two combinations of inlet angle and solidity with the trailing region thickened to 2 and 4 percent chord.

SYMBOLS

c	blade chord, feet
c_d	section drag coefficient
c_l	section lift coefficient
c_{l_0}	camber, expressed as design lift coefficient of isolated airfoil
c_w	wake-momentum-difference coefficient
L/D	lift-drag ratio
P	total pressure, pounds per square foot
p	static pressure, pounds per square foot

q	dynamic pressure, pounds per square foot
R	Reynolds number based on blade chord
S	pressure coefficient, $\left(\frac{P - p_l}{q_1}\right)$
t	maximum section thickness, feet
x	chordwise distance from blade leading edge, feet
y	perpendicular distance from blade chord line, feet
α	angle between the flow direction and the blade chord, degrees
β	angle between the flow direction and the axis, degrees
θ	flow turning angle, degrees ($\beta_1 - \beta_2$)
σ	solidity, chord of blades divided by tangential spacing

Subscripts:

d	design, when used with angles
l	local
1	upstream of blade row
2	downstream of blade row

APPARATUS, PROCEDURE, AND TEST PROGRAM

Apparatus and Procedure

These tests were conducted in the 5-inch low-speed porous-wall cascade tunnel described in references 1 and 2. The improvements in tunnel-wall boundary-layer removal described in reference 1 were also used for these tests. A schematic diagram of the tunnel is given in figure 1. A photograph of the tunnel showing the porous tunnel walls is presented in reference 1.

The testing procedure and methods of calculation used are described in reference 1. The same methods and criteria were used to achieve two-dimensionality of the flow. All nondimensional coefficients are based on the dynamic pressure entering the blade row. The entering velocity

for most of the tests was 95 feet per second and the Reynolds number was 245,000 based on entering velocity and blade chord of 5 inches. For some conditions, usually near design angle of attack, tests were also run at an entering velocity of 135 feet per second and a Reynolds number of 346,000. In addition, some tests near design were made with $\frac{1}{2}$ -inch strips of masking tape placed around the blade leading edges to simulate the effect of leading-edge roughness.

Test Program

Maximum-thickness tests.- The sections tested in the maximum-thickness investigation were the NACA 65-(12)06, 65-(12)08, 65-(12)12, and 65-(12)15 compressor blade sections. Basic thickness forms for NACA 65-series sections of various thicknesses are given on pages 81 to 84 of reference 3. Since these results were to be compared with the data for the NACA 65-(12)10 blade of reference 1, however, a slight additional thickness, increasing linearly along the chord in the same manner as for the NACA 65(216)-010 thickness form in reference 1, was added so direct comparisons could be made. Since the added thickness for the $\frac{t}{c} = 0.10$ sections is given by $\Delta y = 0.0015x$, the basic thickness was increased by the factor $\Delta y = (0.0015x) \left(\frac{t/c}{0.10} \right)$ for sections of other t/c values. As noted in reference 1, the slight differences in basic thicknesses due to the Δy factor are believed to have a negligible effect on performance and the two sets of basic thickness forms are considered to be interchangeable for compressor blades. Ordinates for the blades sections as tested are given in tables I to IV and blade section profiles are presented in figure 2. Maximum-thickness tests were conducted at the three inlet-angle, solidity-combinations $\beta = 45^\circ$, $\sigma = 1.5$ and $\beta = 60^\circ$, $\sigma = 1.0$ and 1.5.

Trailing-edge-thickness tests.- The NACA 65-(12)10 blade section was used in the trailing-edge-thickness tests since this section was considered to be typical of practical camber and thickness. The rearward portion of the basic section was thickened by drawing a straight line tangent to the trailing-edge radii of 1 and 2 percent of the chord and the profile forward of the trailing edge (fig. 3). This method of increasing the trailing-edge thickness is common practice in the industry. The ordinates for the thickened-trailing-edge basic thickness and cambered sections are given in tables V to VII. The effect of the added thickness on the shape of the cambered profiles is shown in figure 4. The 2- and 4-percent trailing-edge-thickness blade was tested at the combinations $\beta = 45^\circ$, $\sigma = 1.5$ and $\beta = 60^\circ$, $\sigma = 1.0$.

RESULTS AND DISCUSSION

Maximum-Thickness Investigation

Surface Pressure Trends and Design Angle-of-Attack Selection:

Surface pressure distribution trends.- The data obtained in the maximum-thickness investigation are presented in figures 5 to 19 in the form of blade-surface pressure distributions and section characteristic curves. The data for the NACA 65(12)10 section given in reference 1 are also presented for ease of comparison. The arrows in the figures designate the design angle of attack selected for the 10-percent-thick sections in reference 1.

The maximum pressure coefficients occurring at any chordwise station are summarized in figure 20 for the three combinations of inlet angle and solidity over the test angle-of-attack range. For the form of pressure coefficient used here, a high value of S corresponds to a high local velocity, that is, to a low local static pressure. Comparison of the pressure coefficients at any given inlet-angle and solidity conditions shows that at the design angle of attack lower maximum pressure coefficients occur on the thinner sections. The highest maximum pressure coefficient at the design angle of attack occurs on the thickest section tested, the NACA 65-(12)15. At angles of attack a few degrees above design, however, the decrease in local static pressure on the convex surface associated with the localized high-speed flow around the leading edge is sufficiently great for the thinner sections with their corresponding smaller leading-edge radii to reverse the trend, so that at angles of attack well above design the thinnest section has the highest maximum pressure coefficient and the thickest section tends to have the lowest. At angles of attack well below the design, the highest pressure coefficient occurs on the concave surface. The general trend at low angles is for the maximum pressure coefficient to increase with increasing thickness.

For angles near positive stall, the maximum pressure coefficients presented in figure 20 appear to again become lower for the smaller thicknesses. This apparent trend may or may not be present. If pressure orifices were installed at very close intervals around the leading edge, the maximum pressure coefficients measured would probably continue to increase with angle of attack at values approaching stall for the thin blades. On the other hand, the existence of high local velocities around a small leading-edge radius would require a very rapid localized pressure recovery which would be conducive to local separation. Possibly, therefore, local separation ahead of the forward orifice relieves the velocity peak by changing the effective blade shape at the leading edge at the expense of increased boundary-layer thickness.

In the pressure distributions of figures 5 to 19 the indications of laminar separation discussed at length in reference 1 are prominent for the thickest sections at angles around the design points.

Selection of design angle of attack.- For high-speed operation, it might appear desirable to select the angle of attack for highest critical Mach number, as indicated by the angle at which the lowest value of maximum pressure coefficient can be obtained, taking into consideration both surfaces. For example, in figure 20(a) this angle for the 6-percent-thick section occurs where the S_{max} curves for the convex and concave surfaces intersect, approximately 10.4° , and equal maximum velocities occur simultaneously on both surfaces. For the 15-percent-thick section, however, this angle occurs at the minimum point of the S_{max} curve for the convex surface, approximately 17.3° . For many of the sections, especially the thinner ones, as in the foregoing example for the 6-percent-thick section, this selection indicates an angle of attack several degrees below the designated design value. However, examination of the individual pressure distributions in figures 5 to 19 shows that the velocity peaks on the concave surface under these conditions are localized peaks. The rapid pressure recovery required downstream of the high local velocity tends to form a thick boundary layer on the concave surface. Furthermore, a localized velocity peak on either surface would be accentuated at high speeds. It thus appears likely that an angle of attack nearer the designated design value would be preferable for high-speed operation in spite of the fact that these low-speed results in some cases indicate slightly higher values of maximum pressure coefficient at that point. In addition, the design angle of attack designated for the 10-percent-thick sections is roughly in the center of the region between the intersection of the S_{max} curves and the points where the slopes of the S_{max} curves for the convex surfaces begin to increase rapidly. In this region, the slopes of the convex surface S_{max} curves are small. Thus, to obtain the widest range of operation, the designated value of α_d from reference 1 is approximately optimum for all t/c values tested.

Section Operating Characteristics:

Turning angle.- That an airfoil in cascade produces less lift than the same profile operating as an isolated airfoil is well known. The reduced lift results from interference between the airfoils in cascade (reference 4). The interference increases as the solidity and the maximum thickness increase. Since turning angle and lift are directly related, the turning angle produced by profiles of given camber would be expected to vary with thickness unless the thickness were small enough to approximate the performance of the ideal thin airfoil.

The curves of turning angle against angle of attack for the sections of various thicknesses are presented in part (g) of figures 5 to 19 and compared for each combination in figure 21. Figure 21 shows that the design turning angles produced are higher for the thinner sections and decrease with increase in maximum thickness. The similarity of the values near design for the 6-percent-thick and 8-percent-thick sections indicate that these sections are essentially operating as ideal thin airfoils, and a further reduction in thickness would not be expected to affect the design turning angle produced. Comparison of figure 21(a) with figure 21(c) shows that interference effects increase more severely with thickness at a higher inlet angle for the same solidity; comparison of figure 21(b) and figure 21(c) confirms that the increase in interference with thickness is more severe for higher solidity at the same inlet angle.

Figures 22 and 23 summarize the effects of thickness on design turning angle for the three combinations. Figure 22(b) indicates the change in design turning angle which can be expected as the maximum profile thickness is varied from 6 percent to 15 percent of the chord. Figure 23 gives the same information in a form which is perhaps more convenient for design use in conjunction with reference 1. Figure 23 indicates the change in camber required to produce the design turning angle indicated for the 10-percent-thick section in the design charts of reference 1 as the maximum thickness is varied.

The velocity over the surface of an airfoil is the sum of incremental velocities due to the profile thickness, camber, and angle of attack. For highly cambered airfoils at angles of attack near design, the incremental velocities due to camber contribute more heavily to the resultant surface velocity than do the incremental velocities due to thickness in the range of thickness investigated herein. For airfoils of less camber than the $c_{l_0} = 1.2$ section used as the basis of comparison, the reverse is probably true. Therefore, the effect of profile thickness on turning angle is expected to be less for more highly cambered sections and greater for sections of less camber than the $c_{l_0} = 1.2$ profiles tested in the present investigation.

Drag.- The curves of wake coefficient and drag coefficient shown in figures 5 to 19 exhibit the irregularities in the region near design discussed in reference 1. These irregularities can be attributed to the effects of laminar separation and turbulent reattachment of the boundary layer. Since exactly the same conditions of Reynolds number, turbulence, and blade-surface condition could hardly be expected to occur in a compressor, no general quantitative conclusions on the effect of maximum thickness on the drag and efficiency can be drawn. Qualitatively, the higher negative pressures occurring on the surfaces of the thicker sections require greater pressure recoveries near the trailing

edges. Greater pressure recovery is conducive to thickening of the boundary layer and increase in drag. Higher wake coefficients were measured near design for the thicker sections. However, the contribution of laminar separation, which may or may not occur in other applications, to these losses cannot be ascertained. The values presented for tests near design at higher Reynolds number and with leading-edge roughness show similar trends and give some idea of the magnitude of the laminar-separation effects. The design turning angles do not appear to be affected by these scale effects within the Reynolds number range of these tests.

Operating range.- As noted previously, the thinner sections have lower maximum pressure coefficients in the region near design, but at angles of attack well above design the smaller leading-edge radii of the thinner sections produce local velocity peaks. Since the amount of turbulent separation near the trailing edge is governed by the boundary-layer condition and the trailing-edge pressure recovery, a severe gradient conducive to boundary-layer growth on the forward portion of the airfoil surface would promote turbulent separation near the trailing edge.

The limits of the useful operating range can be estimated from the observed drag coefficients using Howell's index of twice the minimum drag (reference 5). As discussed previously, accurate values of drag coefficient could not be obtained at angles of attack near design because of laminar separation effects. The minimum drag coefficient could not be determined exactly, so an estimated value was used to determine the operating range. For most of the test configurations, the drag coefficient changed rapidly near the ends of the useful range, so an error in the value of minimum drag would have only a small effect on the estimated operating range. Using Howell's index, the operating range increases about 50 percent as the section thickness increases from 6 percent to 15 percent chord. There should be no laminar separation effects on the stalling characteristics since at either end of the range the pressure distribution on the pertinent surface is not conducive to laminar flow.

In a compressor two conditions which might well modify the conclusions on operating range have not been reproduced in these tests. At speeds near the critical, the deleterious effects of velocity peaks on the critical Mach number for angles of attack just a few degrees from design might reduce the effective operating range well below that for the low-speed tests; in the compressor, the angle of attack and inlet angle change together, in contrast to the cascade tested in which the angle of attack was varied at constant inlet angle, thus giving different relations between pressure rise and angle of attack for the two configurations.

Predicted critical Mach number.- The pressure rise obtained from a given axial compressor is proportional to the square of the operating Mach number. The variation of critical Mach number, that is, the entering Mach number at which sonic velocities first appear on the blade surface, with thickness is therefore of considerable interest. Fairly reliable prediction of the critical Mach number for isolated airfoils can be made from low-speed tests from charts such as the one given on page 114 of reference 3. Such a chart is not directly applicable to airfoils in cascade because the change in "free stream velocity" from upstream to downstream makes difficult the choice of the correct stream Mach number to use with the chart. If the peak velocity occurred at the very leading edge, however, it seems logical that the upstream Mach number would be the correct one to use in the prediction. For conditions under which the peak velocity occurs near the airfoil leading edge, perhaps within the first 20 percent of the chord, the critical Mach number estimated on the basis of the upstream Mach number should be useful for comparison purposes. The prediction of critical speed trends with thickness variation at design angle of attack has been made on that basis and is given in figure 24. Slight differences usually occur between the normal-force coefficients obtained by integrating the blade-surface pressure distributions and normal-force coefficients calculated using measured pressure and momentum changes across the cascade. Correcting the pressure distribution so that the integrated normal force agrees with that calculated from momentum and pressure changes yields more consistent critical Mach number trends. This correction was made in calculating the values presented in figure 24. For this reason, the measured S_{max} values of figure 20 do not agree exactly with the M_{cr} values in figure 24.

On the basis of the low-speed tests, only a small change in critical speed at design is shown in figure 24 as the maximum thickness is varied from 6 to 12 percent of the chord. As the thickness is increased to 15 percent, the reduction in critical speed becomes more noticeable. Because the local velocities at design angle of attack are the sum of the contributions of thickness and camber, more pronounced effects would be expected with sections of lower camber, and less effect would be expected with sections of higher camber. The trend of the more important criterion, force-break Mach number, with thickness variation, cannot be predicted from low-speed tests, but the trends are presumed to be at least somewhat similar to those for critical speed. In any event, the values of force-break Mach number can be expected to be above those shown for critical speed in figure 24.

Trailing-Edge-Thickness Investigation

The section characteristics of the NACA 65-(12)10 compressor blade having a 1- and 2-percent-chord trailing-edge radius are given in figures 25 and 26 for the conditions $\beta = 45^\circ$, $\sigma = 1.5$ and $\beta = 60^\circ$, $\sigma = 1.0$. For comparison with the NACA 65-(12)10 section having the usual 0.15-percent trailing-edge radius, figures 7(g) and 12(g) may be referred to, respectively. At design angles of attack, the section having a 1-percent trailing-edge radius produced a turning angle less by only 0.2° at $\beta = 45^\circ$, $\sigma = 1.5$ and less by about 0.6° at $\beta = 60^\circ$, $\sigma = 1.0$ and the section having a 2-percent trailing-edge radius produced a turning less by 1.0° at $\beta = 45^\circ$, $\sigma = 1.5$ and less by 0.6° at $\beta = 60^\circ$, $\sigma = 1.0$ than the section having a 0.15-percent trailing-edge radius. The drag coefficients observed were not sensibly affected by the changes in trailing-edge radius. A 1-percent trailing-edge radius is probably sufficient from structural or vibrational considerations. Although the effects of trailing-edge thickness would probably be different for other cambers, inlet angles, or solidities, the section having a 1-percent trailing-edge radius will probably perform similarly to the sections reported in reference 1. For these reasons, the use of a 1-percent-chord trailing-edge radius with compressor blade sections of 10-percent-chord maximum thickness is recommended for practical construction.

CONCLUSIONS

NACA 65-series compressor blades cambered to an isolated airfoil lift coefficient of 1.2 have been tested in a low-speed porous-wall cascade with maximum section thicknesses of 6, 8, 10, 12, and 15 percent of the chord. These sections were tested over the useful angle-of-attack range at inlet angle, β , and solidity, σ , combinations of $\beta = 45^\circ$, $\sigma = 1.5$ and $\beta = 60^\circ$, $\sigma = 1.0$ and 1.5. A 10-percent-thick section tested with a trailing-edge radius of 1 and 2 percent chord was compared with data for a similar section having the usual 0.15-percent-chord trailing-edge radius. This section was tested at inlet angle and solidity combinations of $\beta = 45^\circ$, $\sigma = 1.5$ and $\beta = 60^\circ$, $\sigma = 1.0$. From the results of these investigations, the following conclusions were reached.

1. Changing the section thickness from 6 percent to 15 percent chord did not significantly affect the design angle of attack selected on the basis of previous tests of the NACA 65-(12)10 compressor blade section.

2. As the section thickness was increased from 6 to 15 percent chord, the design turning angle decreased 2° at inlet angle, solidity

combinations of $\beta = 45^\circ$, $\sigma = 1.5$ and $\beta = 60^\circ$, $\sigma = 1.0$ and about 4° at $\beta = 60^\circ$, $\sigma = 1.5$.

3. The pressure coefficients for the 6-percent-thick section are generally lower than those of thicker sections at angles of attack from below design to a few degrees above design; at higher angles of attack, thicker sections have lower pressure coefficients.

4. The critical Mach number of these sections at design angle of attack, estimated using the Karman-Tsien extrapolation, decreased about 0.02 at $\beta = 60^\circ$, $\sigma = 1.0$ and 1.5 and about 0.05 at $\beta = 45^\circ$, $\sigma = 1.5$ as the thickness was increased from 6 percent to 15 percent chord.

5. The operating range based on Howell's index increased about 50 percent in these low-speed tests as the section thickness was increased from 6 to 15 percent chord.

6. Sections having trailing-edge radii equal to 10 percent of the maximum section thickness are recommended for practical construction.

Langley Aeronautical Laboratory
National Advisory Committee for Aeronautics
Langley Field, Va.

REFERENCES

1. Herrig, L. Joseph, Emery, James C., and Erwin, John R.: Systematic Two-Dimensional Cascade Tests of NACA 65-Series Compressor Blades at Low Speeds. NACA RM L51G31, 1951.
2. Erwin, John R., and Emery, James C.: Effect of Tunnel Configuration and Testing Technique on Cascade Performance. NACA Rep. 1016, 1951. (Formerly NACA TN 2028.)
3. Abbott, Ira H., Von Doenhoff, Albert E., and Stivers, Louis S., Jr.: Summary of Airfoil Data. NACA Rep. 824, 1945. (Formerly NACA ACR L5C05.)
4. Katzoff, S., Finn, Robert S., and Laurence, James C.: Interference Method for Obtaining the Potential Flow past an Arbitrary Cascade of Airfoils. NACA Rep. 879, 1947. (Formerly NACA TN 1252.)
5. Howell, A. R.: Design of Axial Compressors. Lectures on the Development of the British Gas Turbine Jet Unit Published in War Emergency Issue No. 12 of the Institution of Mechanical Engineers. A.S.M.E. Reprint, Jan. 1947, pp. 452-462.

TABLE I

COORDINATES FOR THE NACA 65-(12)06 COMPRESSOR BLADE SECTION

[Stations and ordinates in percent of chord]

Upper surface		Lower surface	
x	y	x	y
0	0	0	0
.285	.725	.715	-.125
.507	.941	.993	-.101
.974	1.305	1.527	-.021
2.184	2.020	2.816	.212
4.644	3.163	5.356	.630
7.128	4.096	7.872	.992
9.624	4.896	10.376	1.308
14.639	6.219	15.362	1.857
19.672	7.254	20.328	2.298
24.716	8.075	25.284	2.665
29.768	8.702	30.232	2.962
34.824	9.159	35.176	3.201
39.883	9.458	40.118	3.394
44.942	9.594	45.058	3.547
50.00	9.563	50.00	3.673
55.054	9.361	54.946	3.780
60.100	8.996	59.900	3.856
65.135	8.481	64.864	3.879
70.161	7.823	69.839	3.842
75.173	7.023	74.827	3.717
80.171	6.070	79.829	3.482
85.154	4.968	84.846	3.109
90.121	3.680	89.879	2.524
95.058	2.167	94.942	1.626
100.03	.0847	99.970	-.0847

L.E. radius: 0.240
Slope of radius through L.E.: 0.505

TABLE II

COORDINATES FOR THE NACA 65-(12)08 COMPRESSOR BLADE SECTION

[Stations and ordinates in percent of chord]

Upper surface		Lower surface	
x	y	x	y
0	0	0	0
.217	.861	.783	-.261
.430	1.106	1.070	-.266
.885	1.516	1.615	-.232
2.081	2.315	2.919	-.083
4.526	3.582	5.474	.210
7.004	4.612	7.996	.476
9.498	5.494	10.502	.710
14.518	6.947	15.482	1.129
19.562	8.083	20.438	1.469
24.621	8.979	25.379	1.761
29.690	9.661	30.310	2.004
34.765	10.153	35.235	2.207
39.843	10.469	40.157	2.383
44.923	10.597	45.077	2.543
50.0	10.535	50.00	2.701
55.071	10.273	54.929	2.867
60.132	9.823	59.868	3.020
65.108	9.224	64.820	3.136
70.213	8.460	69.787	3.204
75.228	7.544	74.772	3.196
80.225	6.474	79.775	3.078
85.202	5.254	84.798	2.822
90.159	3.858	89.842	2.347
95.099	2.248	94.901	1.544
100.041	.113	99.959	-.113

L.E. radius: 0.434
Slope of radius through L.E.: 0.505



TABLE III

COORDINATES FOR THE NACA 65-(12)12 COMPRESSOR BLADE SECTION

[Stations and ordinates in percent of chord]

Upper surface		Lower surface	
x	y	x	y
0	0	0	0
.083	1.125	.917	-.525
.281	1.426	1.219	-.586
.715	1.924	1.785	-.640
1.879	2.893	3.121	-.661
4.292	4.413	5.708	-.621
6.757	5.642	8.243	-.554
9.247	6.669	10.753	-.485
14.267	8.434	15.724	-.358
19.343	9.744	20.658	-.192
24.431	10.791	25.569	-.051
29.534	11.583	30.466	+.081
34.648	12.145	35.352	.215
39.765	12.490	40.235	.362
44.884	12.599	45.116	.541
50.00	12.465	50.00	.771
55.106	12.080	54.894	1.060
60.196	11.473	59.805	1.379
65.265	10.670	64.735	1.690
70.312	9.688	69.688	1.976
75.333	8.547	74.667	2.193
80.327	7.244	79.673	2.309
85.292	5.797	84.709	2.279
90.228	4.187	89.772	2.017
95.143	2.403	94.857	1.389
100.061	.169	99.939	-.169

L.E. radius: 1.000
Slope of radius through L.E.: 0.505



TABLE IV

COORDINATES FOR THE NACA 65-(12)15 COMPRESSOR BLADE SECTION

[Stations and ordinates in percent of chord]

Upper surface		Lower surface	
x	y	x	y
0	0	0	0
-.007	1.304	1.007	-.704
.176	1.651	1.324	-.811
.593	2.216	1.907	-.932
1.730	3.315	3.270	-1.083
4.119	5.031	5.881	-1.239
6.572	6.410	8.428	-1.322
9.060	7.583	10.940	-1.379
14.095	9.501	15.906	-1.425
19.178	10.990	20.822	-1.438
24.288	12.153	25.712	-1.413
29.417	13.028	30.583	-1.364
34.554	13.642	35.441	-1.282
39.706	14.009	40.294	-1.157
44.856	14.097	45.144	-.957
50.000	13.899	50.000	-.663
55.131	13.413	54.869	-.273
60.242	12.675	59.758	.177
65.327	11.720	64.673	.818
70.384	10.574	69.616	1.090
75.409	9.262	74.591	1.479
80.399	7.788	79.601	1.764
85.355	6.177	84.645	1.899
90.277	4.420	89.723	1.784
95.174	2.514	94.826	1.278
100.102	.201	99.898	-.201

L.E. radius: 1.505
Slope of radius through L.E.: 0.505



TABLE V
 COORDINATES FOR THE NACA 65-010 COMPRESSOR BLADE SECTION
 HAVING 1- AND 2-PERCENT-CHORD TRAILING-EDGE RADII
 [Stations and ordinates in percent of chord]

Stations, x	Ordinates, y	
	1-percent T.E.R.	2-percent T.E.R.
0	0	0
.5	.752	.752
.75	.890	.890
1.25	1.124	1.124
2.5	1.571	1.571
5.0	2.222	2.222
7.5	2.709	2.709
10	3.111	3.111
15	3.746	3.746
20	4.218	4.218
25	4.570	4.570
30	4.824	4.824
35	4.982	4.982
40	5.057	5.057
45	5.029	5.029
50	4.870	4.870
55	4.570	4.574
60	4.175	4.275
65	3.768	3.976
70	3.362	3.677
75	2.955	3.378
80	2.549	3.080
85	2.142	2.781
90	1.735	2.482
95	1.329	2.183
100	0	0
T.E.R.	1.00	2.00



TABLE VI

COORDINATES FOR NACA 65-(12)10 COMPRESSOR BLADE SECTION

HAVING A TRAILING-EDGE RADIUS OF 1 PERCENT CHORD

[Stations and ordinates in percent of chord]

Upper surface		Lower surface	
x	y	x	y
0	0	0	0
.161	.971	.839	-.371
.374	1.227	1.126	-.387
.817	1.679	1.683	-.395
1.981	2.599	3.019	-.367
4.399	4.035	5.601	-.243
6.868	5.178	8.132	-.090
9.361	6.147	10.639	.057
14.388	7.734	15.612	.342
19.477	8.958	20.553	.594
24.523	9.915	25.477	.825
29.611	10.640	30.389	1.024
34.706	11.153	35.294	1.207
39.804	11.479	40.196	1.373
44.904	11.598	45.096	1.542
50.000	11.488	50.000	1.748
55.087	11.139	54.913	2.001
60.162	10.598	59.838	2.254
65.222	9.941	64.778	2.419
70.271	9.183	69.729	2.481
75.308	8.309	74.692	2.431
80.334	7.303	79.666	2.249
85.350	6.151	84.650	1.925
90.356	4.800	89.644	1.404
95.360	3.175	94.640	.617
100.000	0	100.000	0

L.E. radius: 0.666
Slope of radius through L.E.: 0.505
T.E. radius: 1.0
Slope of radius through T.E.: -0.505



TABLE VII

COORDINATES FOR NACA 65-(12)10 COMPRESSOR BLADE SECTION

HAVING A TRAILING-EDGE RADIUS OF 2 PERCENT CHORD

[Stations and ordinates in percent of chord]

Upper surface		Lower surface	
x	y	x	y
0	0	0	0
.161	.971	.839	-.371
.374	1.227	1.126	-.387
.817	1.679	1.683	-.395
1.981	2.599	3.019	-.367
4.399	4.035	5.601	-.243
6.868	5.178	8.132	-.090
9.361	6.147	10.639	.057
14.388	7.734	15.612	.342
19.477	8.958	20.553	.594
24.523	9.915	25.477	.825
29.611	10.640	30.389	1.024
34.706	11.153	35.294	1.207
39.804	11.479	40.196	1.373
44.904	11.598	45.096	1.542
50.000	11.488	50.000	1.748
55.087	11.143	54.913	1.997
60.166	10.698	59.835	2.154
65.234	10.149	64.766	2.211
70.296	9.497	69.704	2.167
75.351	8.730	74.649	2.010
80.401	7.829	79.599	1.723
85.449	6.782	84.551	1.294
90.499	5.531	89.501	.673
95.569	3.997	94.431	-.205
100.000	0	100.000	0

L.E. radius: 0.666
Slope of radius through L.E.: 0.505
T.E. radius: 2.0
Slope of radius through T.E.: -0.505



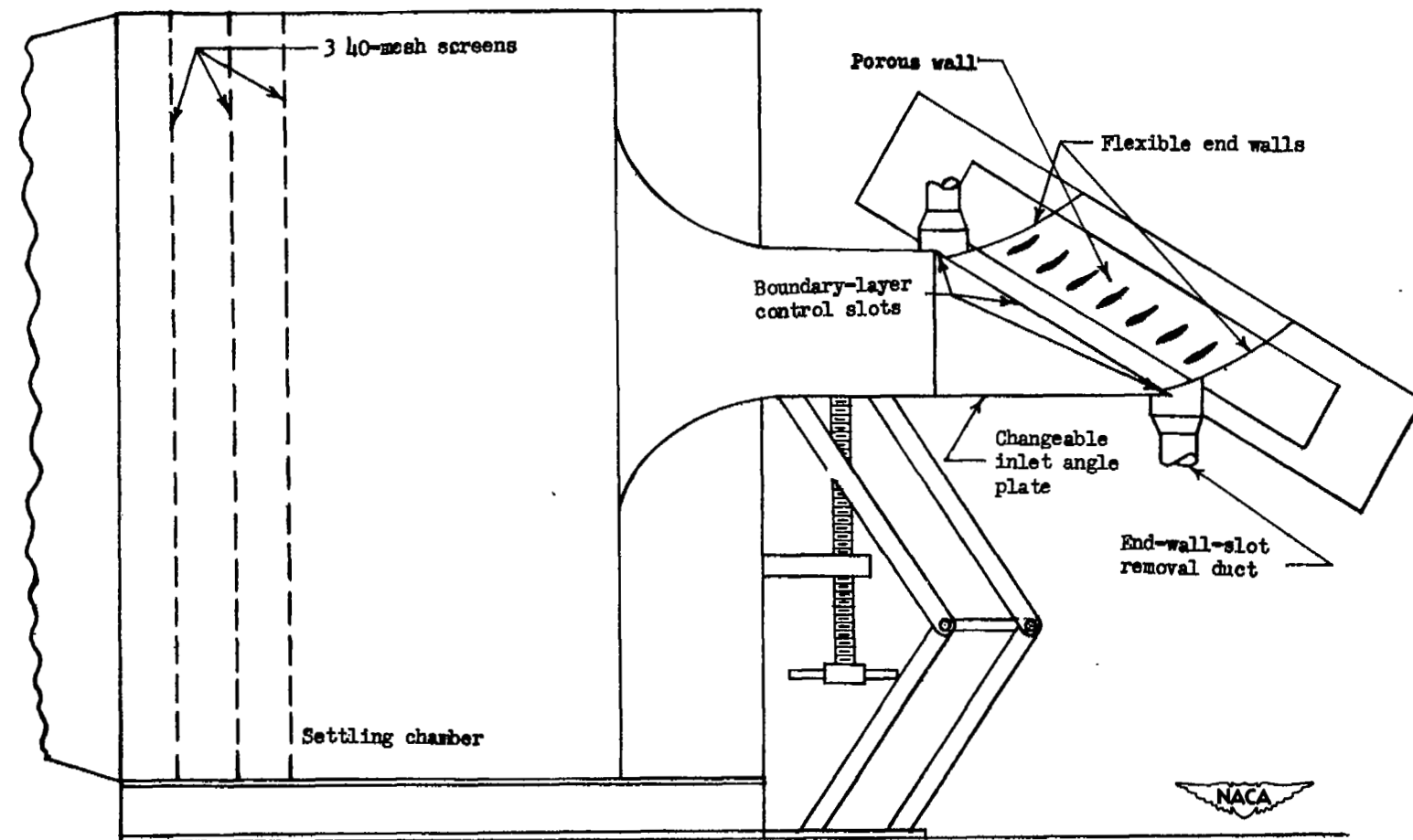
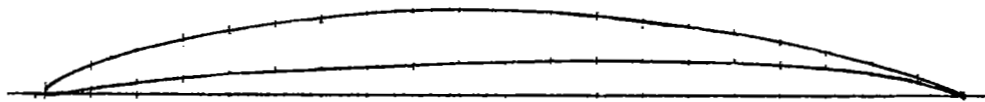
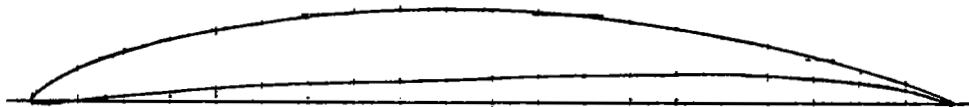


Figure 1.- Vertical cross section of two-dimensional low-speed cascade tunnels.



65-(12)06



65-(12)08



65-(12)10



65-(12)12



65-(12)15

Figure 2.- Comparison of blade sections having different maximum thickness.

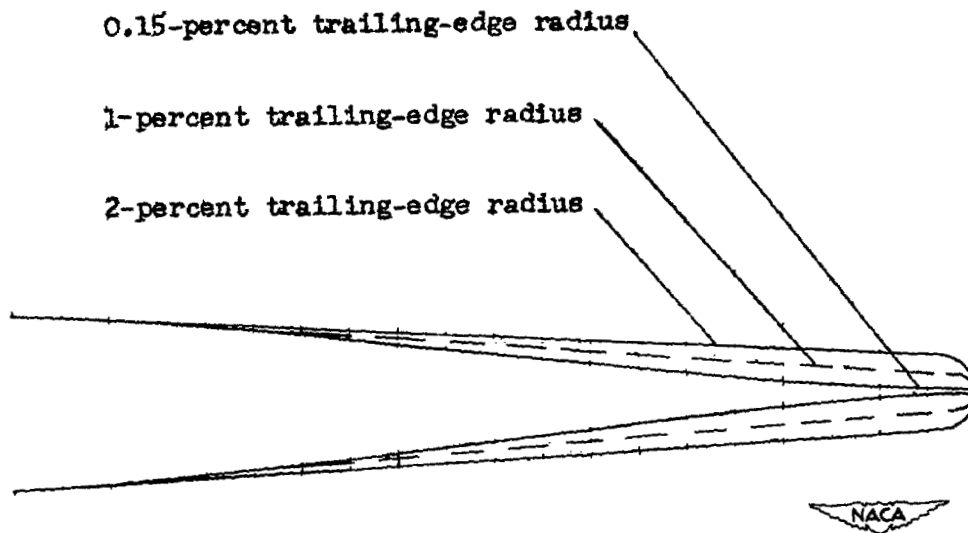
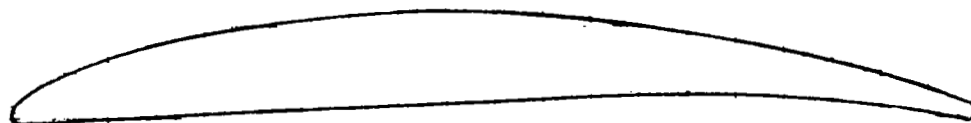
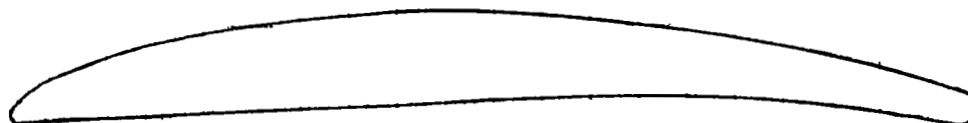


Figure 3.- NACA 65-010 basic thickness sections having 0.15-percent, 1-percent, and 2-percent-chord trailing-edge radius.



1-percent trailing-edge radius



2-percent trailing-edge radius



Figure 4.- NACA 65-(12)10 compressor blade sections having 1-percent and 2-percent trailing-edge radius.

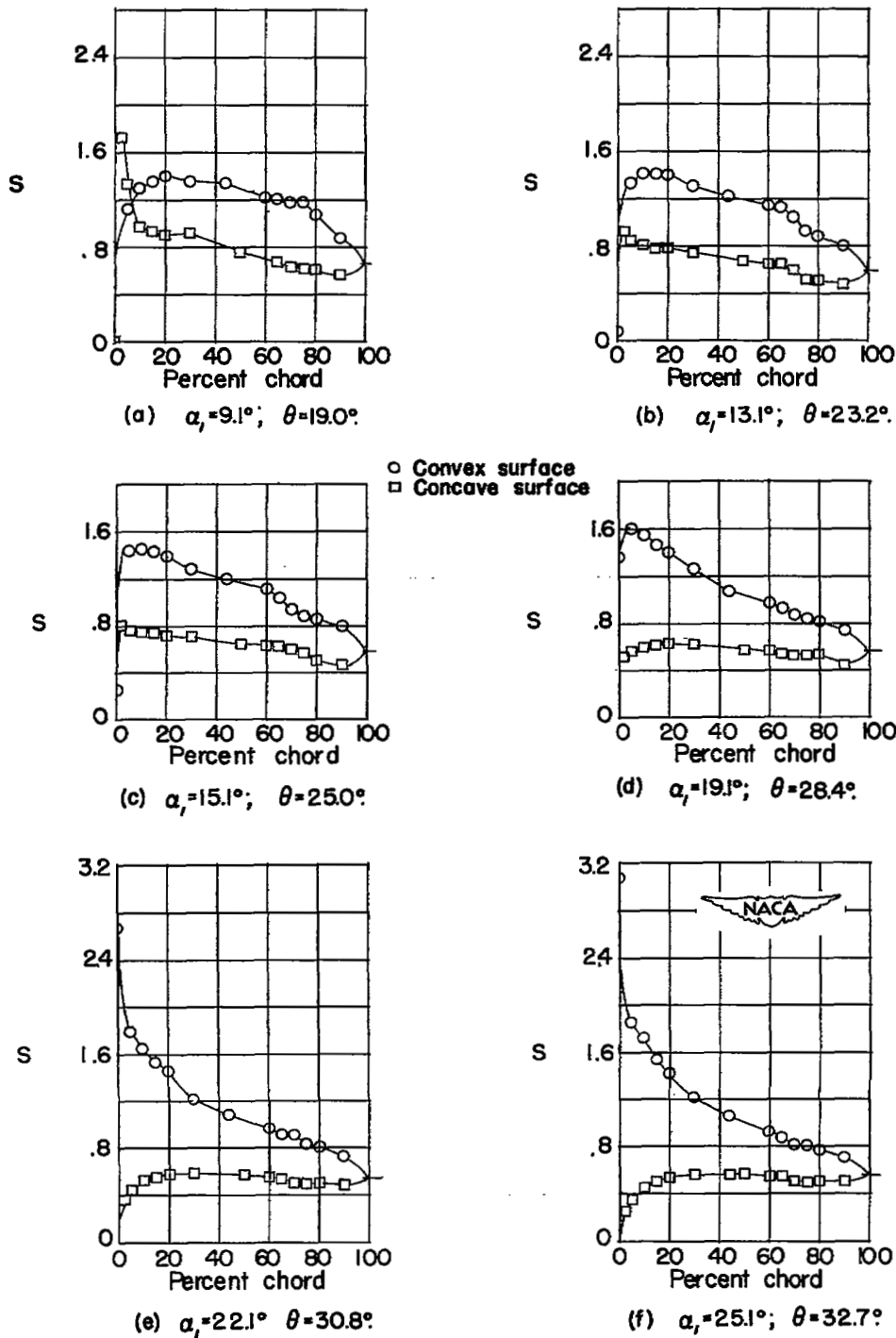
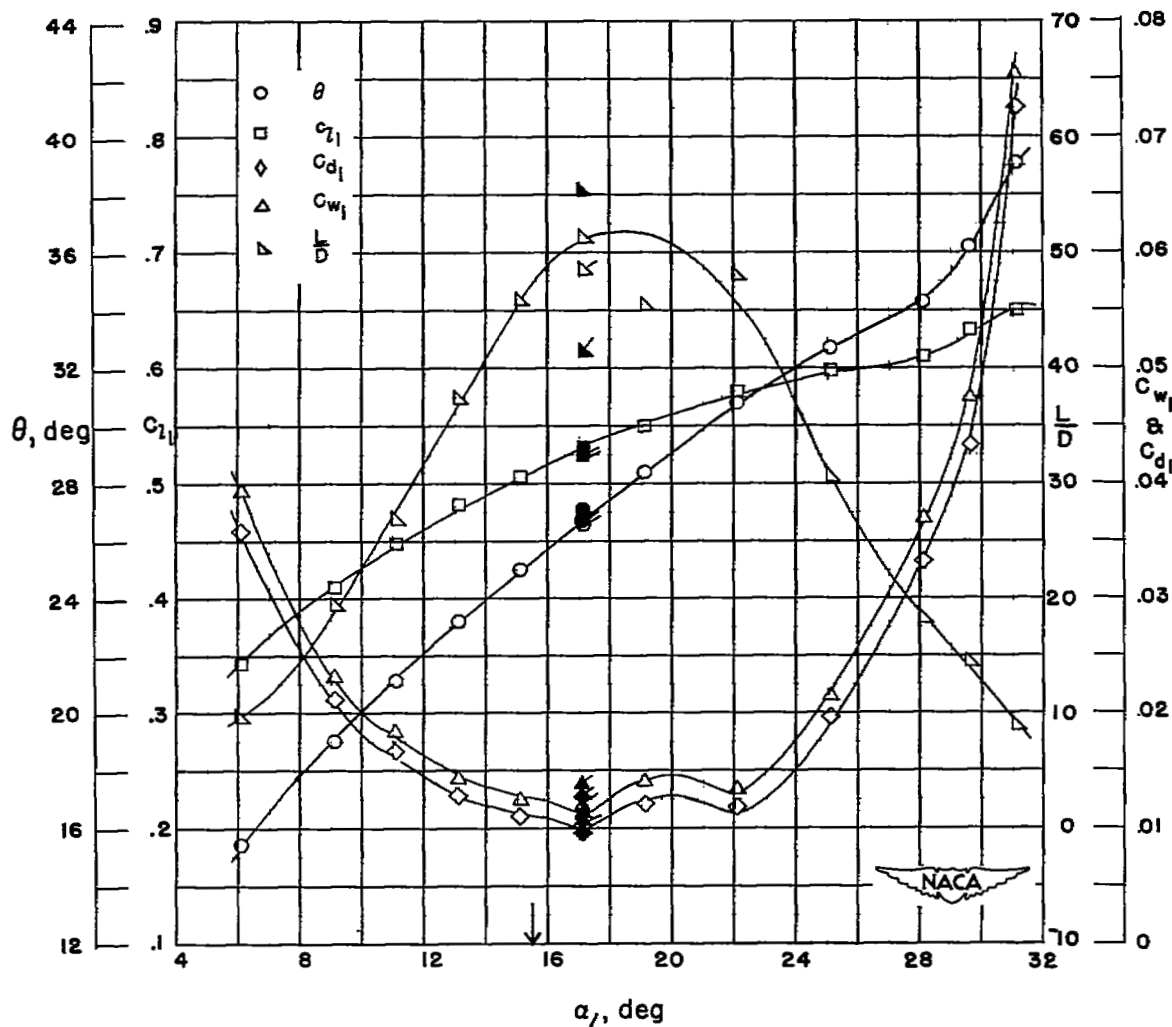


Figure 5.- Blade-surface pressure distributions and blade section characteristics for the cascade combination, $\beta_1 = 45^\circ$, $\sigma = 1.50$, and blade section, 65-(12)06.

4F



(g) Section characteristics; arrow shows design angle of attack; flagged symbol indicates leading-edge roughness; solid symbol indicates high Reynolds number.

Figure 5.- Concluded.

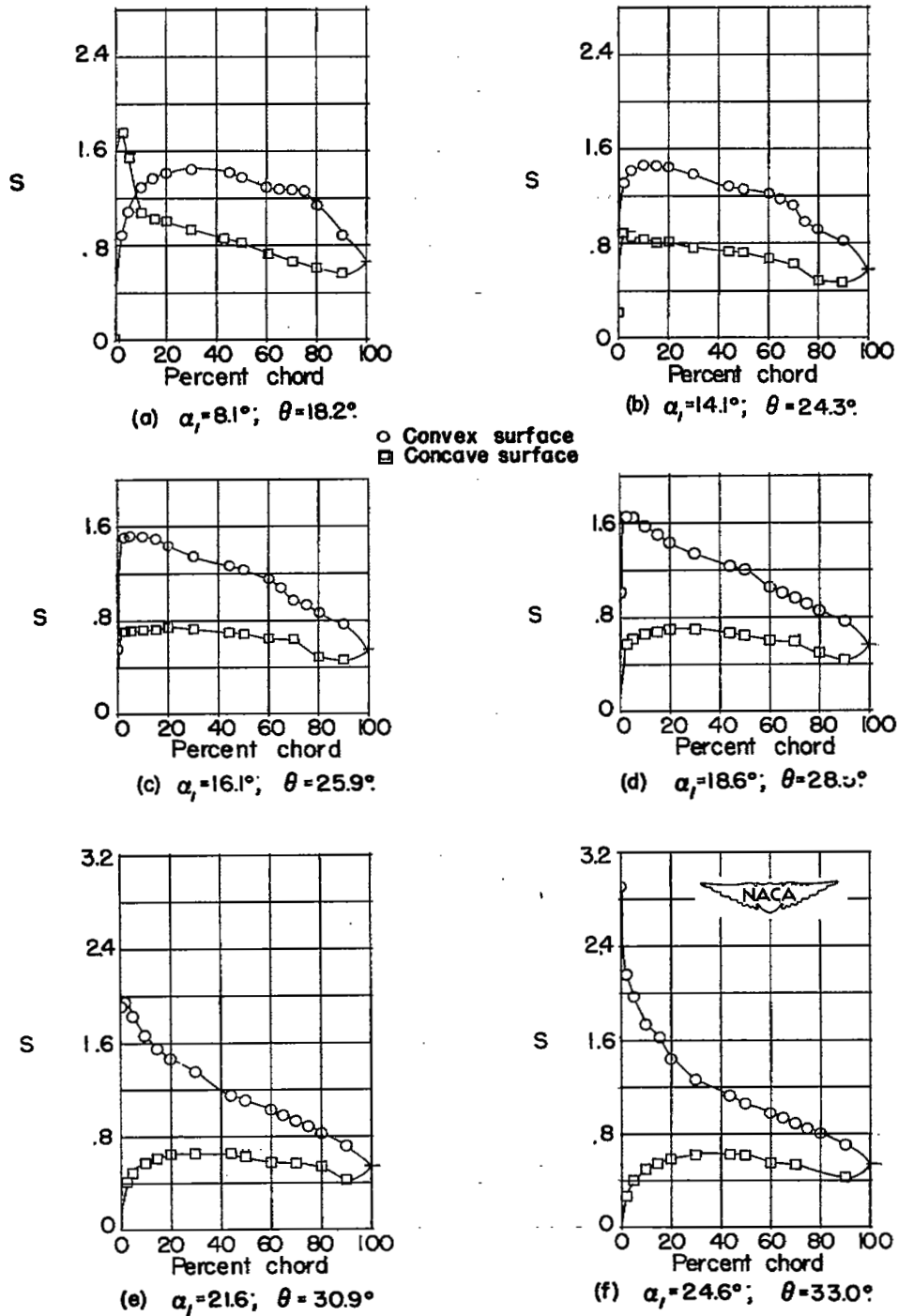
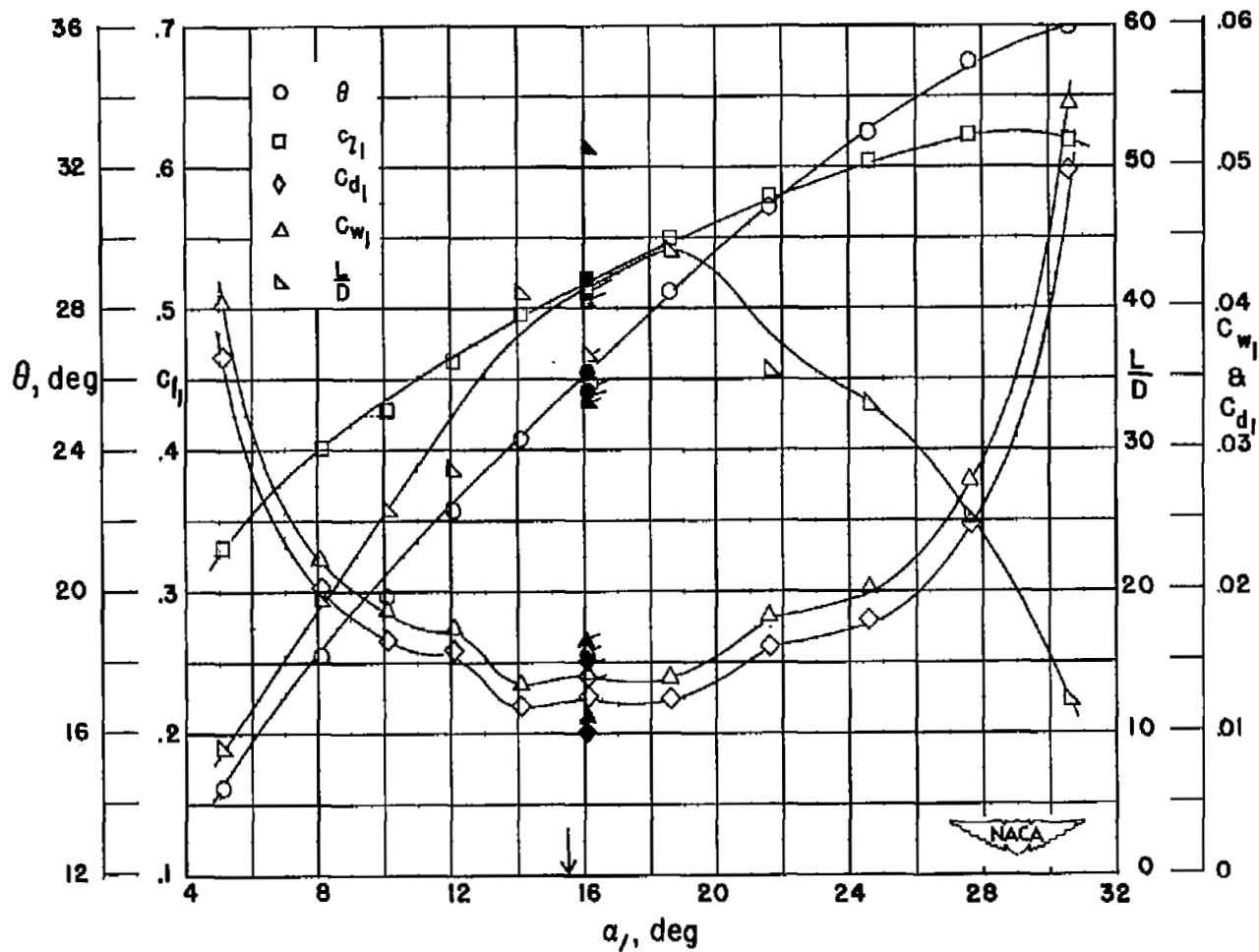


Figure 6.- Blade-surface pressure distributions and blade section characteristics for the cascade combination, $\beta_1 = 45^\circ$, $\sigma = 1.50$, and blade section, 65-(12)08.



(g) Section characteristics; arrow shows design angle of attack; flagged symbol indicates leading-edge roughness; solid symbol indicates high Reynolds number.

Figure 6.- Concluded.

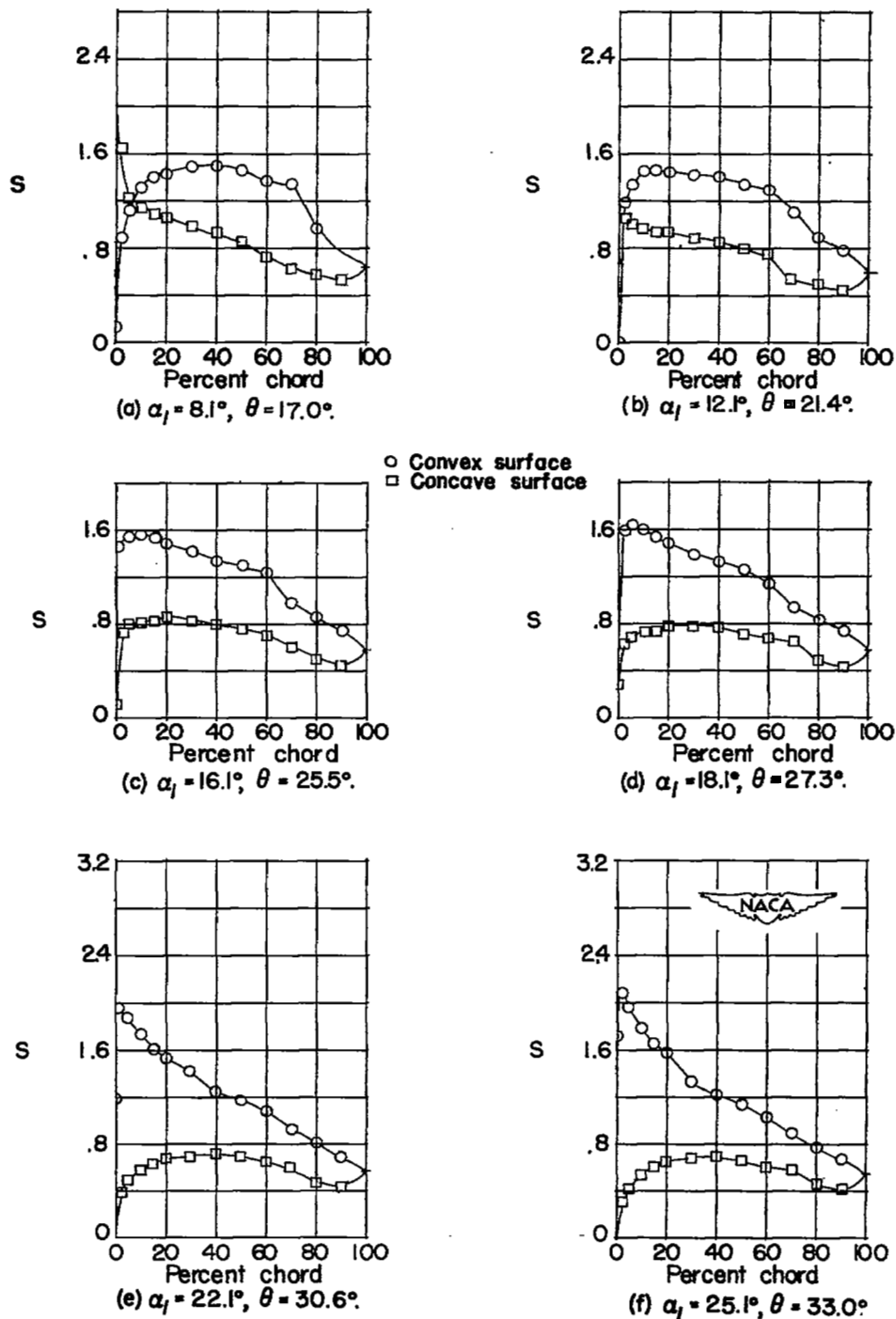
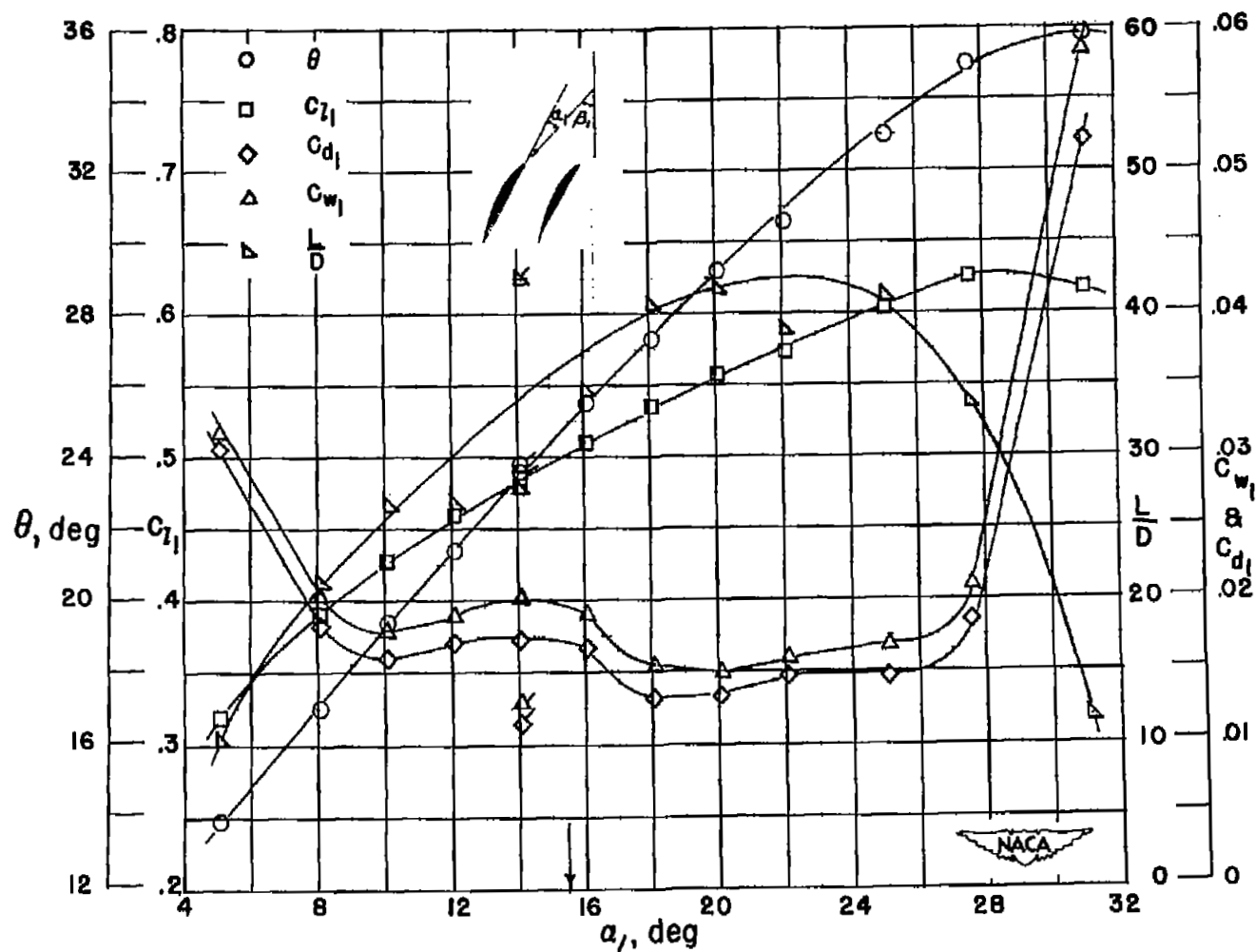


Figure 7.- Blade-surface pressure distributions and blade section characteristics for the cascade combination, $\beta_1 = 45^\circ$, $\sigma = 1.50$, and blade section, 65-(12)10.



(g) Section characteristics; arrow shows design angle of attack, flagged symbol indicates leading-edge roughness

Figure 7.- Concluded.

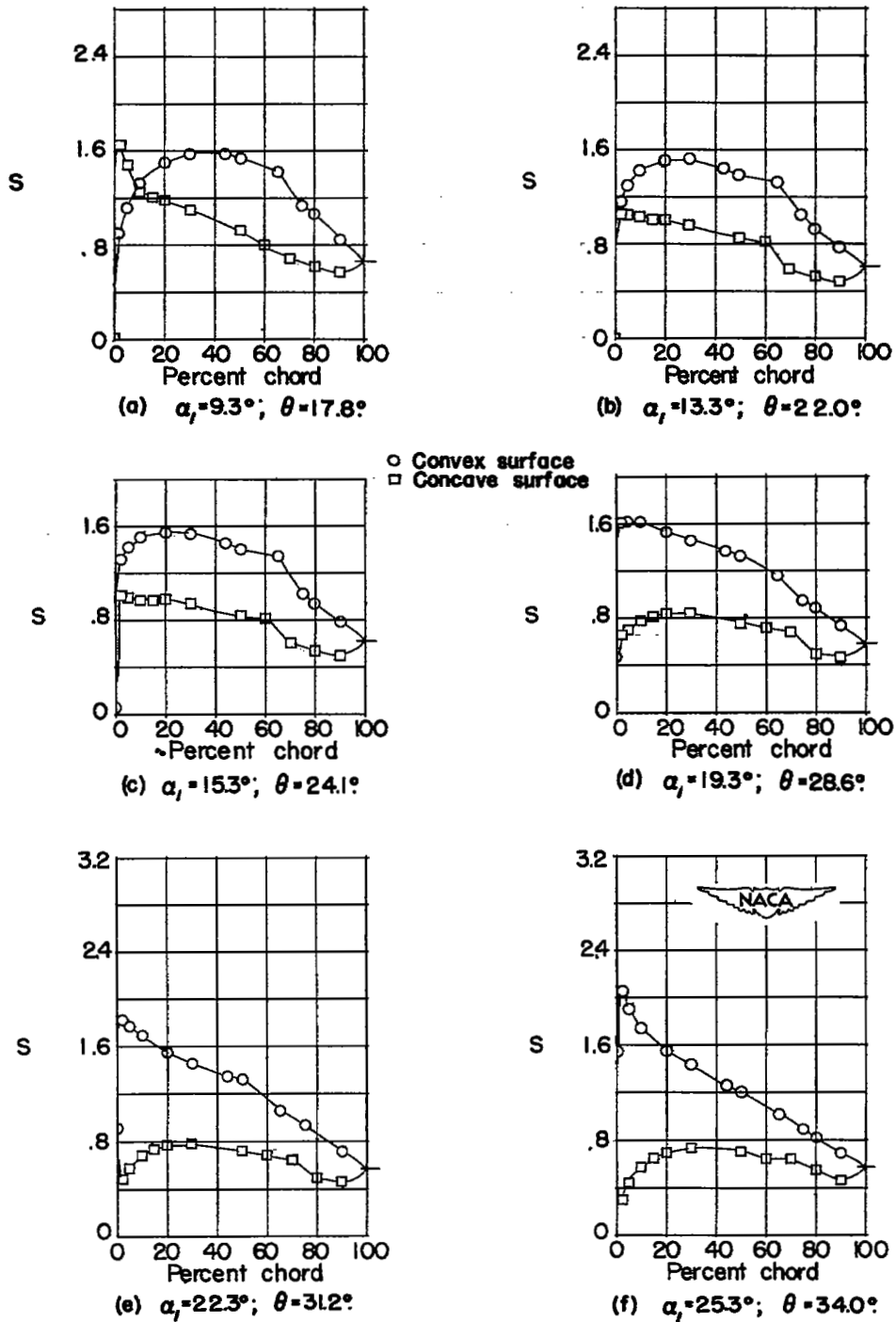
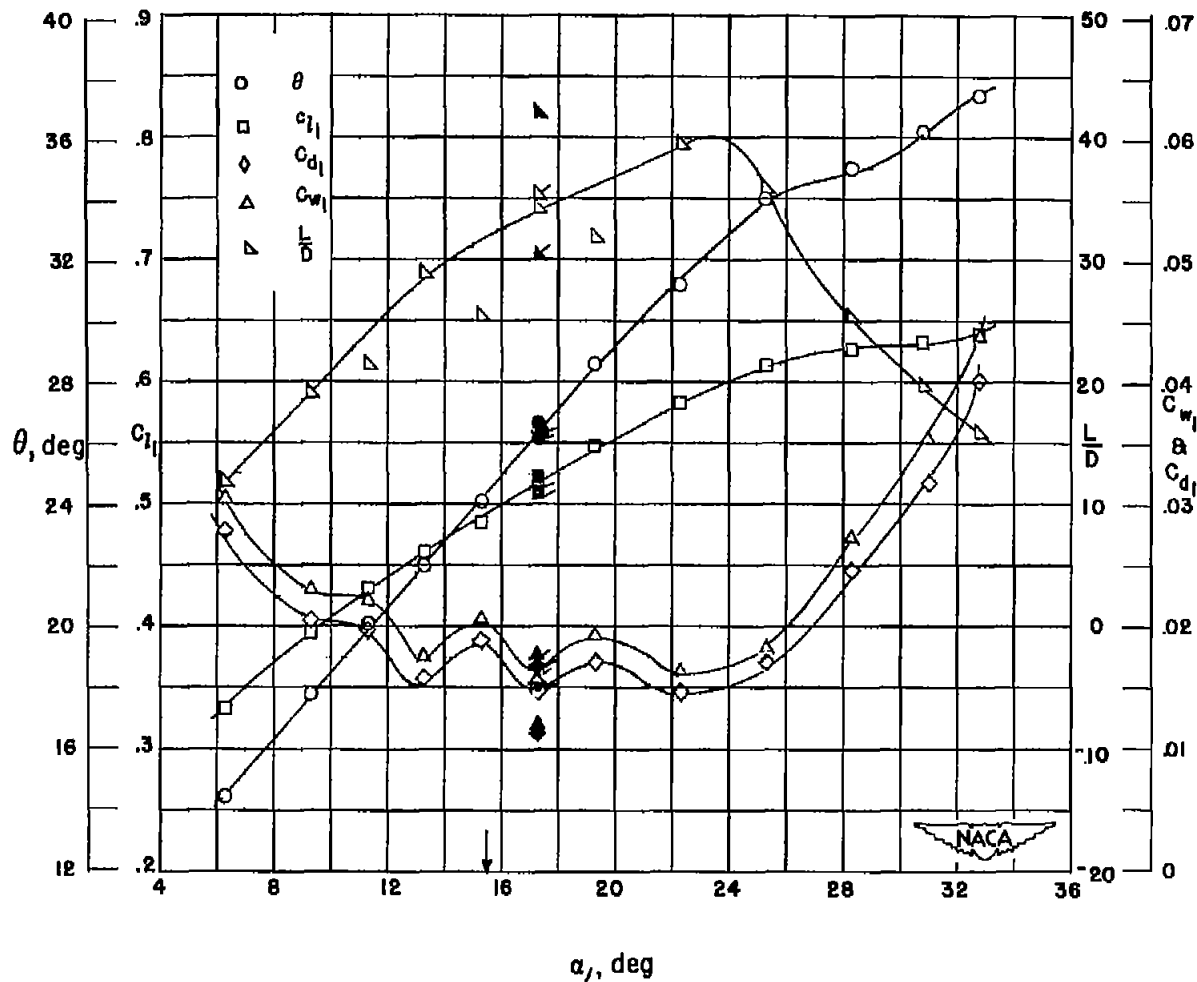


Figure 8.- Blade-surface pressure distributions and blade section characteristics for the cascade combination, $\beta_1 = 45^\circ$, $\sigma = 1.50$, and blade section, 65-(12)12.



(g) Section characteristics; arrow shows design angle of attack; flagged symbol indicates leading-edge roughness; solid symbol indicates high Reynolds number.

Figure 8.- Concluded.

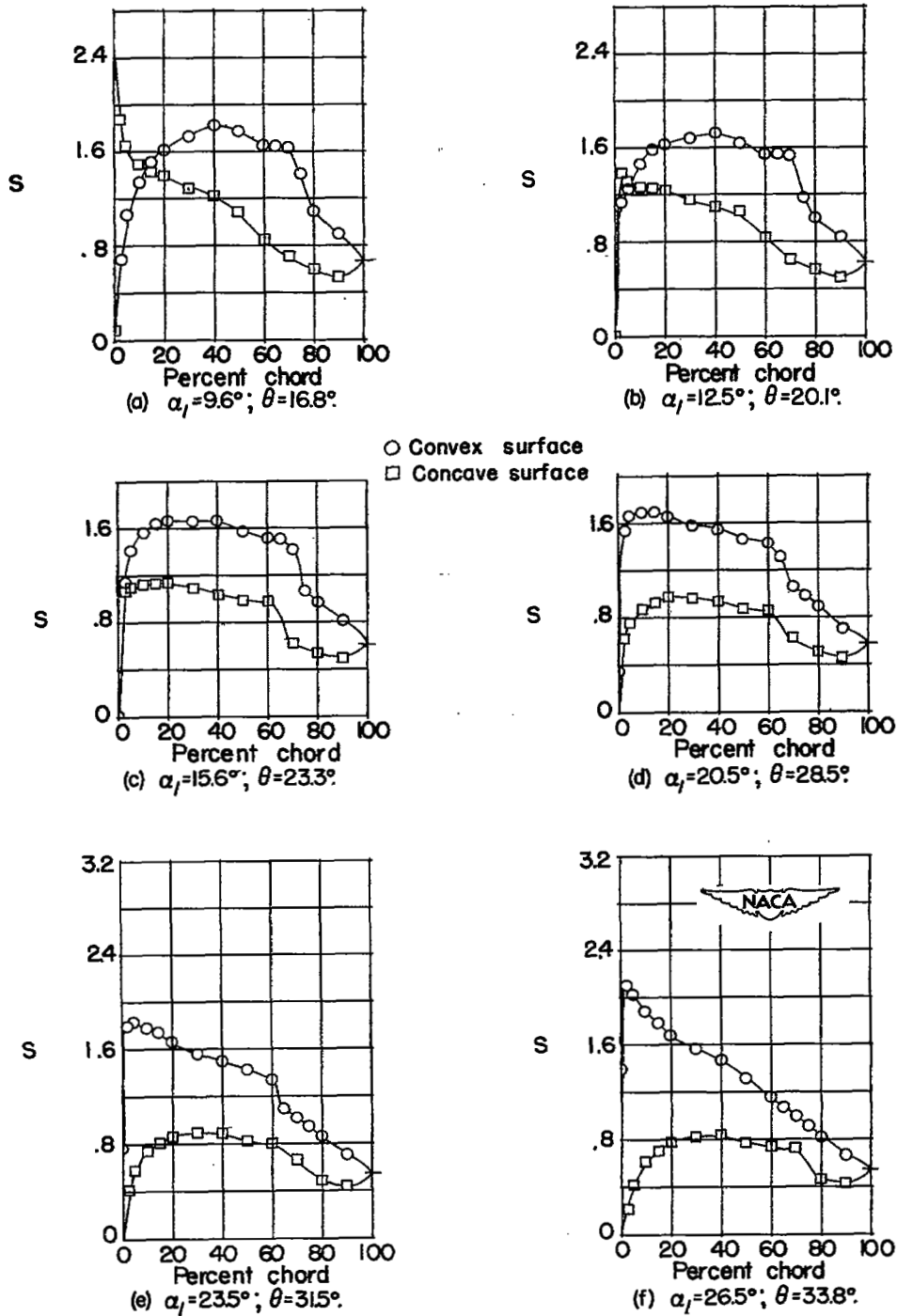
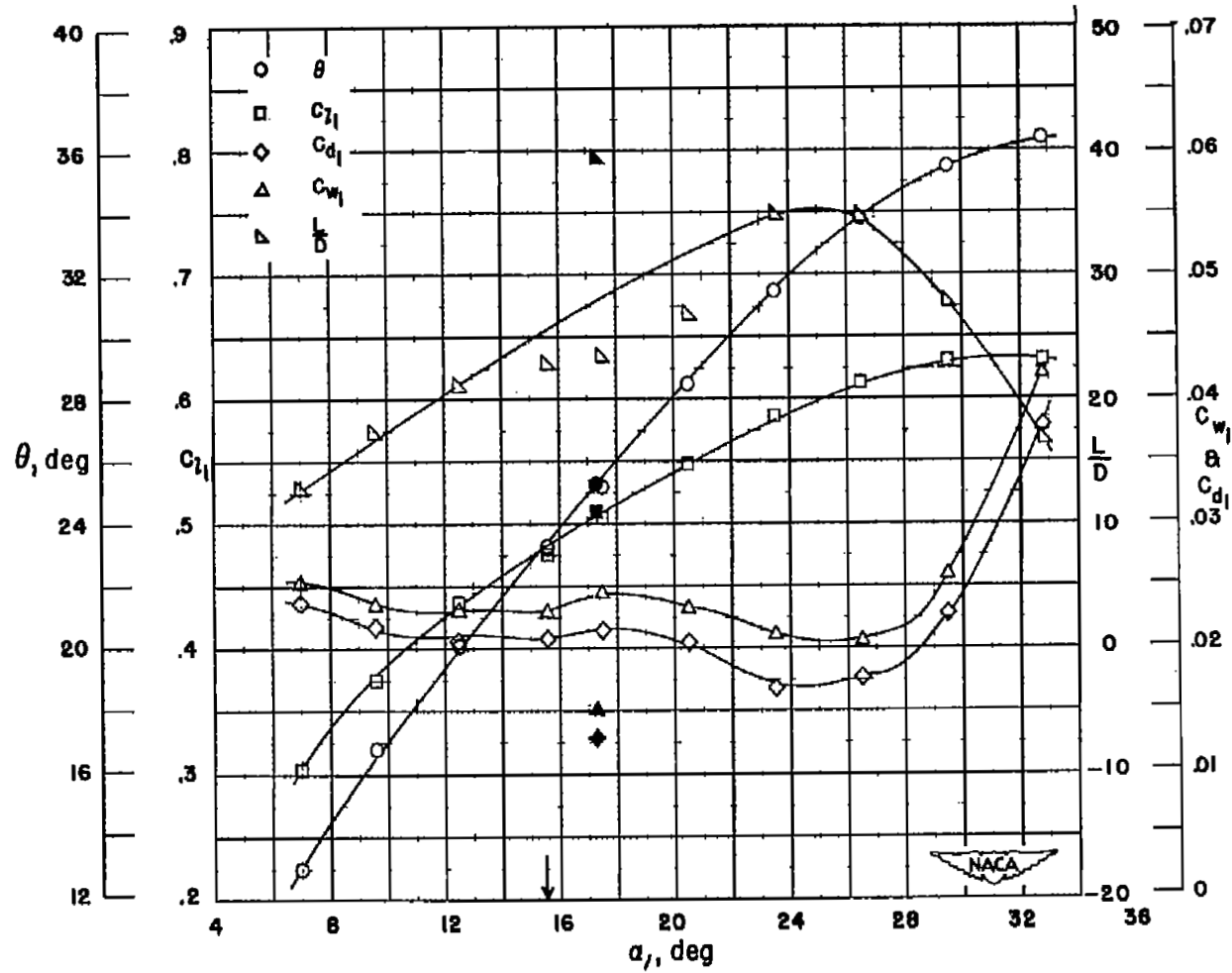


Figure 9.- Blade-surface pressure distributions and blade section characteristics for the cascade combination, $\beta_1 = 45^\circ$, $\sigma = 1.50$, and blade section, 65-(12)15.



(g) Section characteristics; arrow shows design angle of attack, flagged symbol indicates leading-edge roughness, solid symbol indicates high Reynolds number.

Figure 9.- Concluded.

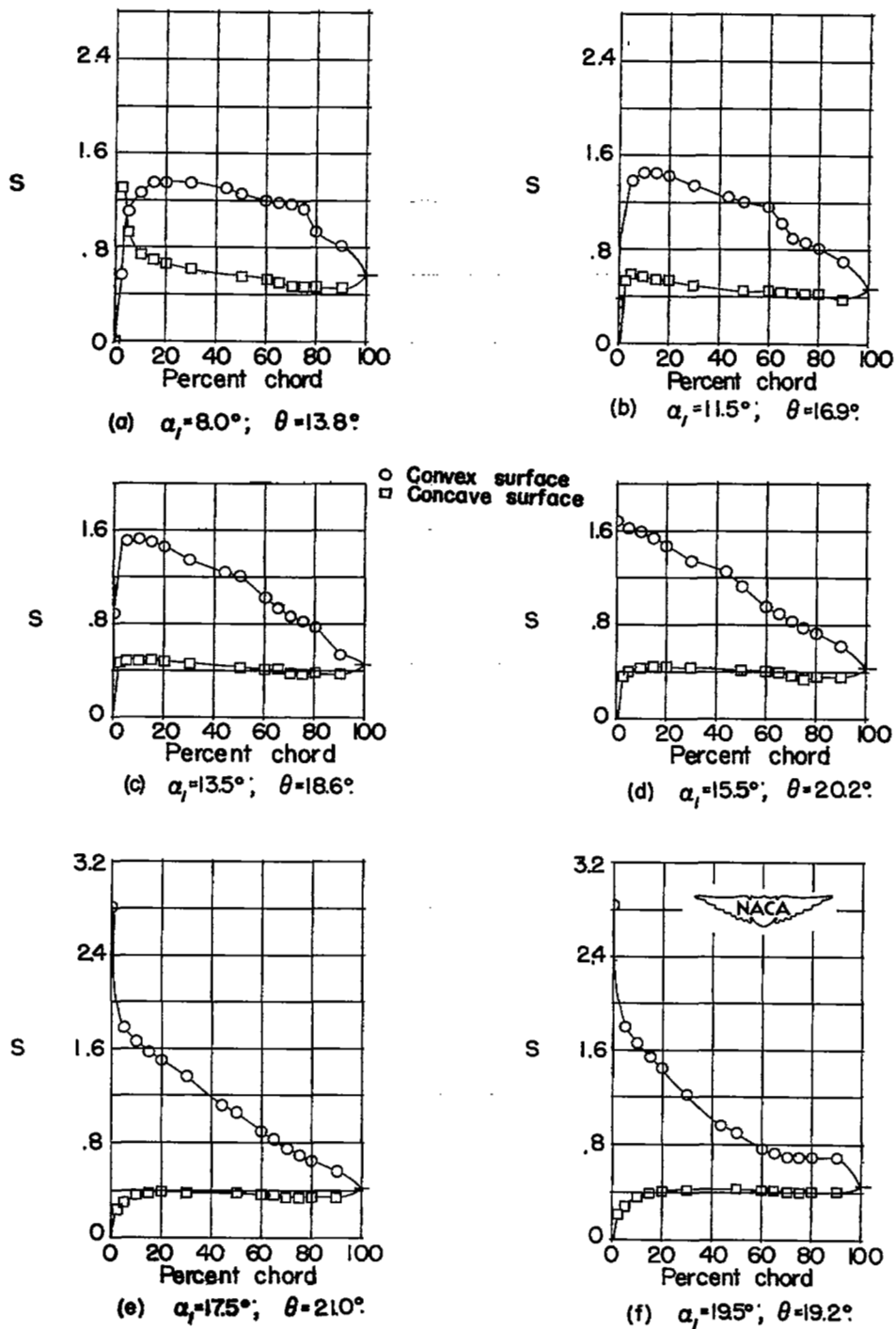
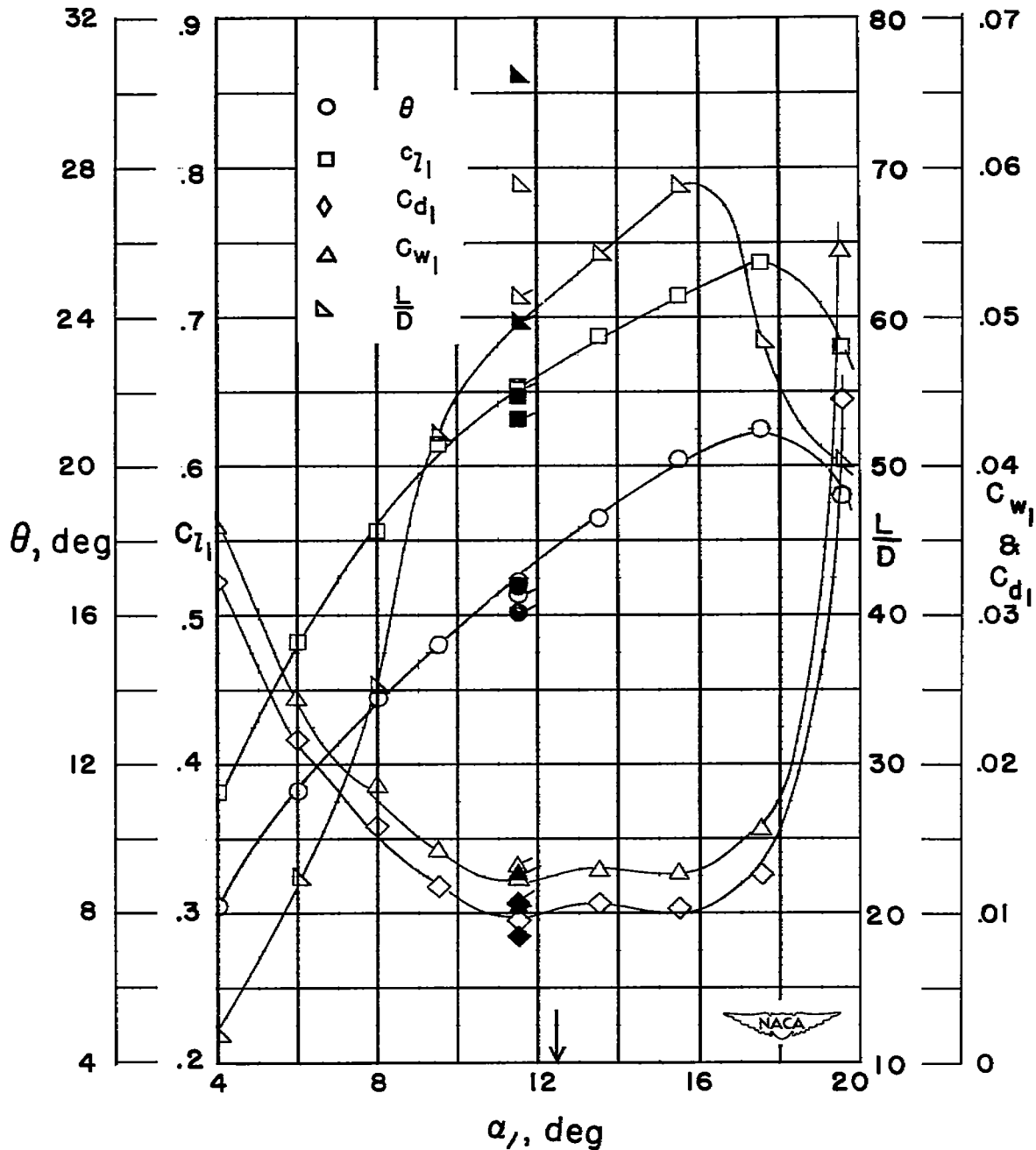


Figure 10.- Blade-surface pressure distributions and blade section characteristics for the cascade combination, $\beta_1 = 60^\circ$, $\sigma = 1.00$, and blade section, 65-(12)06.



(g) Section characteristics; arrow shows design angle of attack; flagged symbol indicates leading-edge roughness; solid symbol indicates high Reynolds number.

Figure 10.- Concluded.

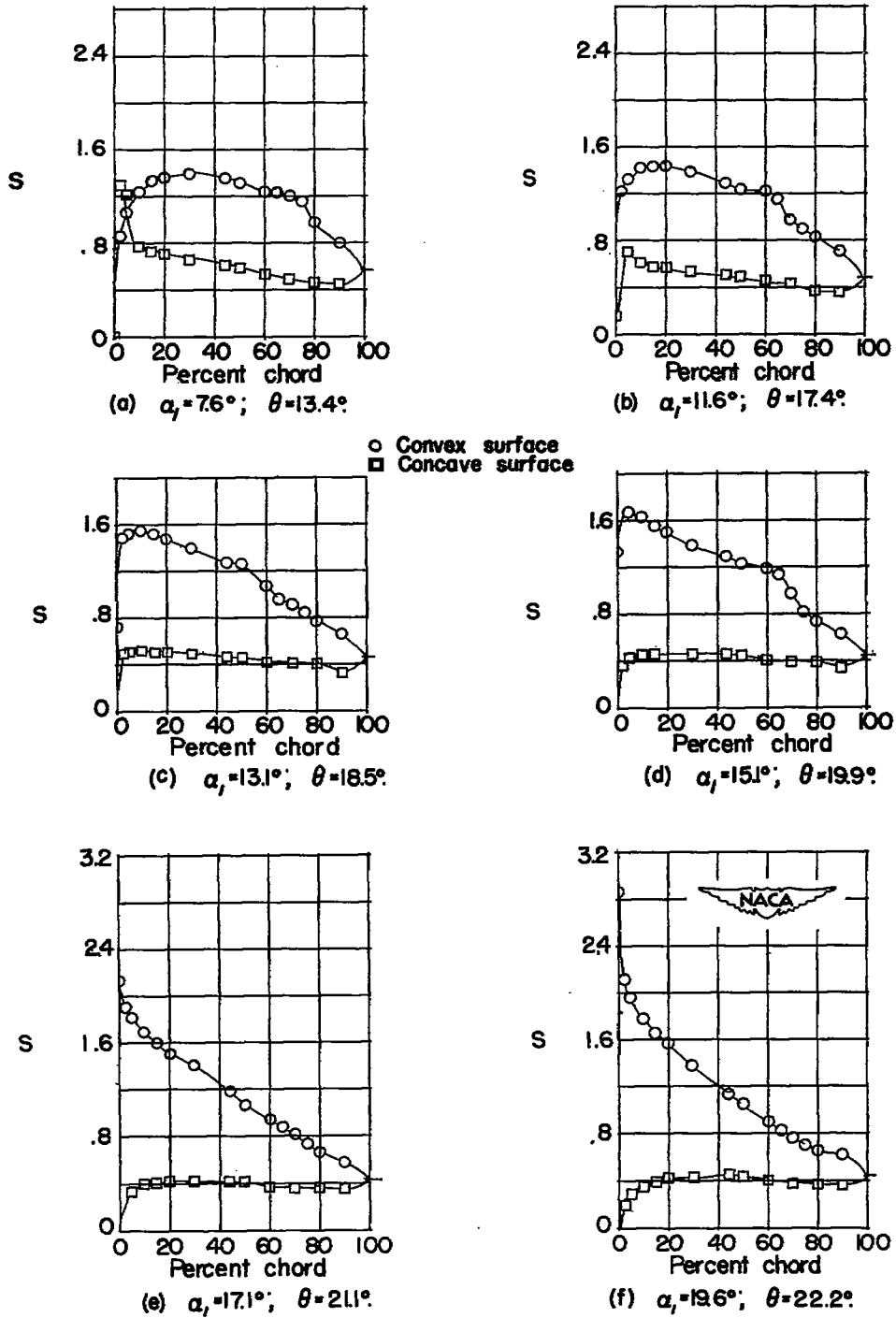
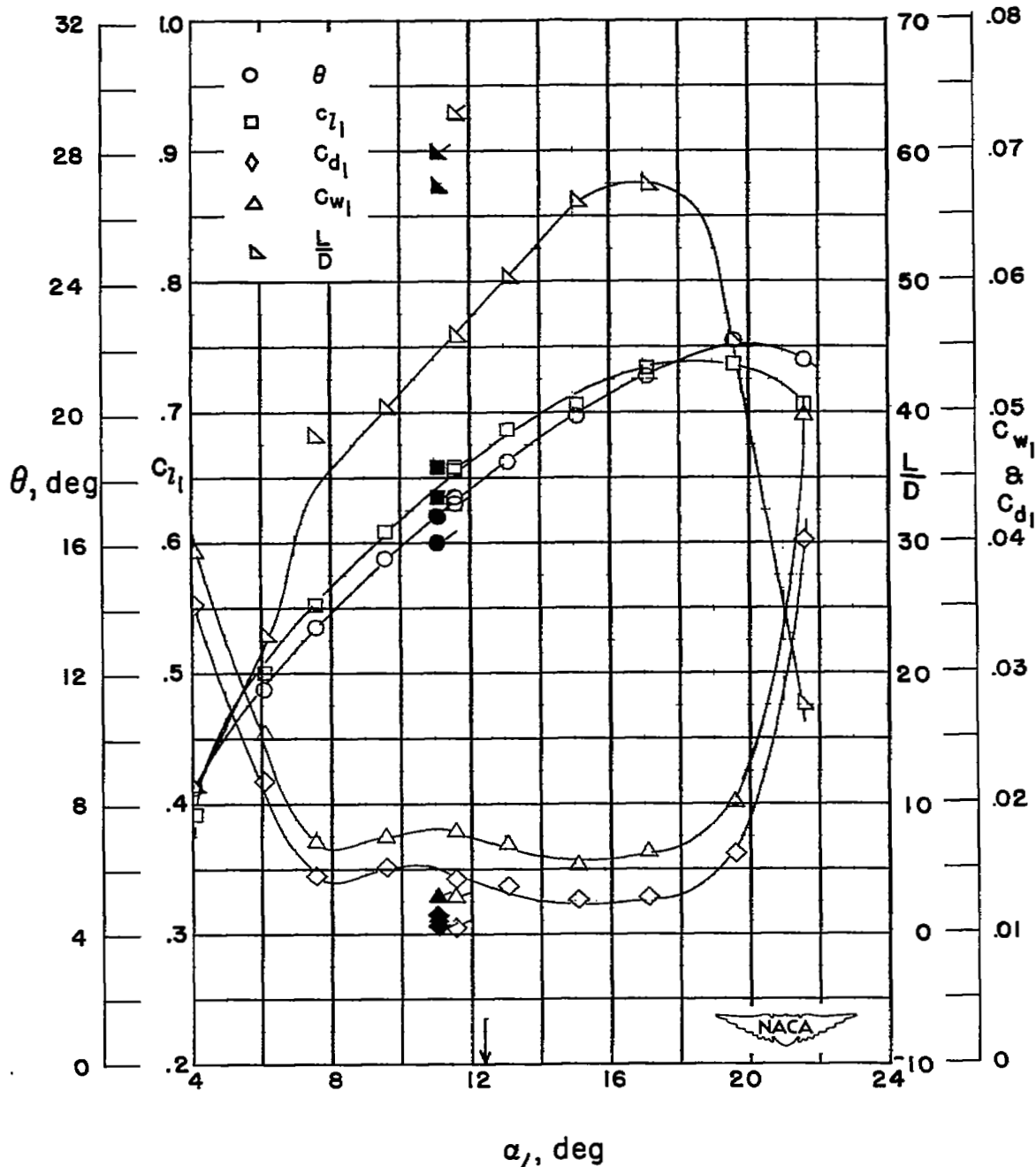


Figure 11.- Blade-surface pressure distributions and blade section characteristics for the cascade combination, $\beta_1 = 60^\circ$, $\sigma = 1.00$, and blade section, 65-(12)08.



(g) Section characteristics; arrow shows design angle of attack; flagged symbol indicates leading-edge roughness; solid symbol indicates high Reynolds number.

Figure 11.- Concluded.

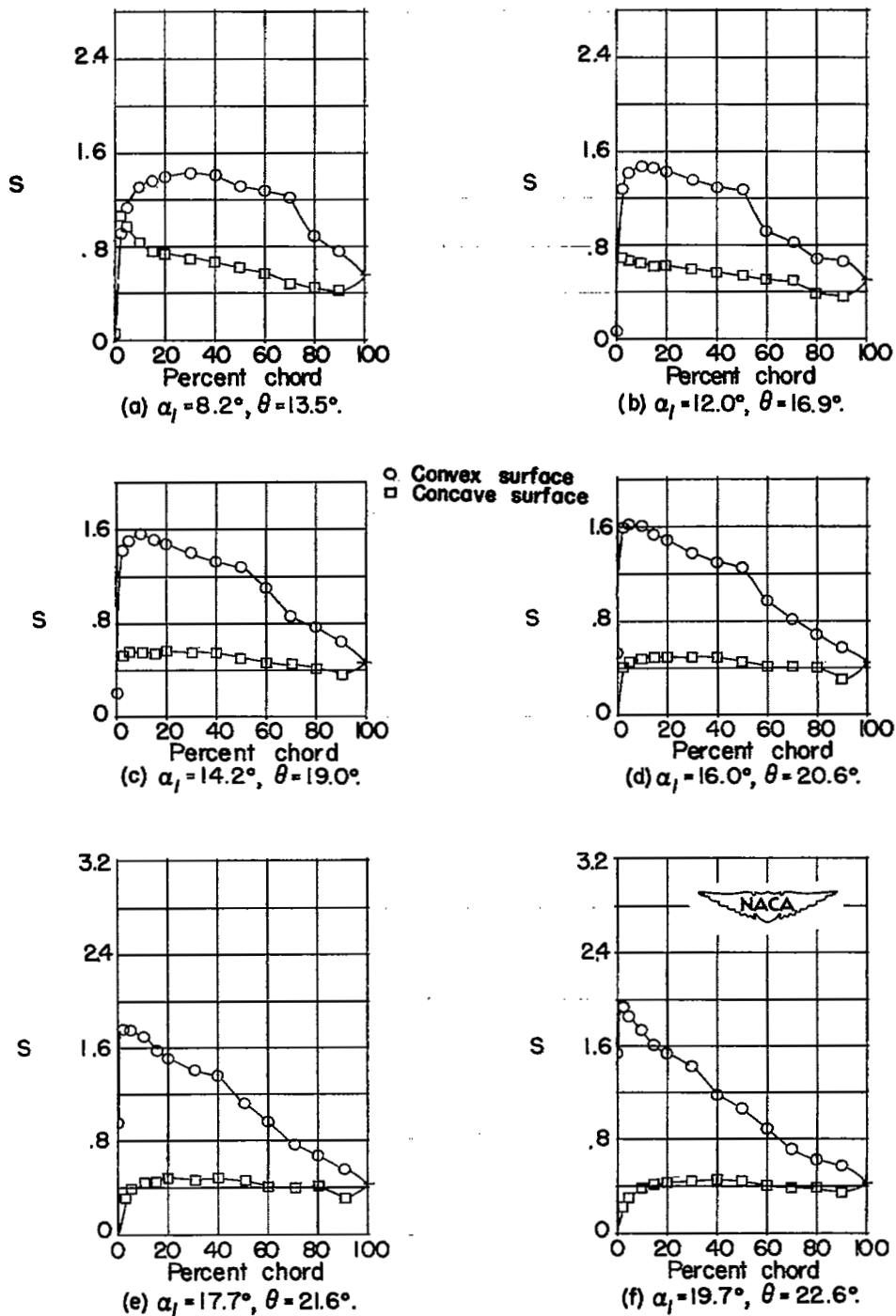
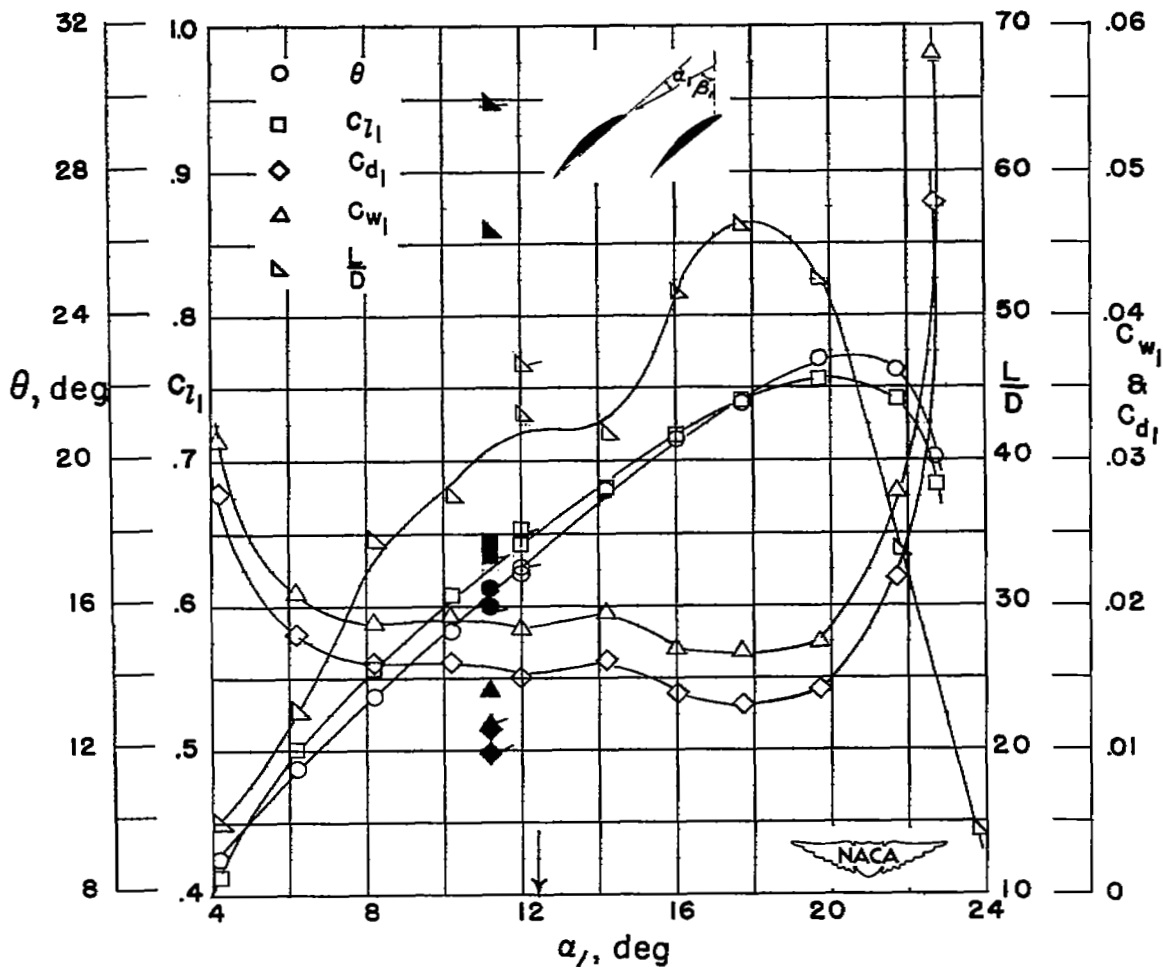


Figure 12.- Blade-surface pressure distributions and blade section characteristics for the cascade combination, $\beta_1 = 60^\circ$, $\sigma = 1.00$, and blade section, 65-(12)10.



(g) Section characteristics; arrow shows design angle of attack; flagged symbol indicates leading-edge roughness; solid symbol indicates high Reynolds number.

Figure 12.- Concluded.

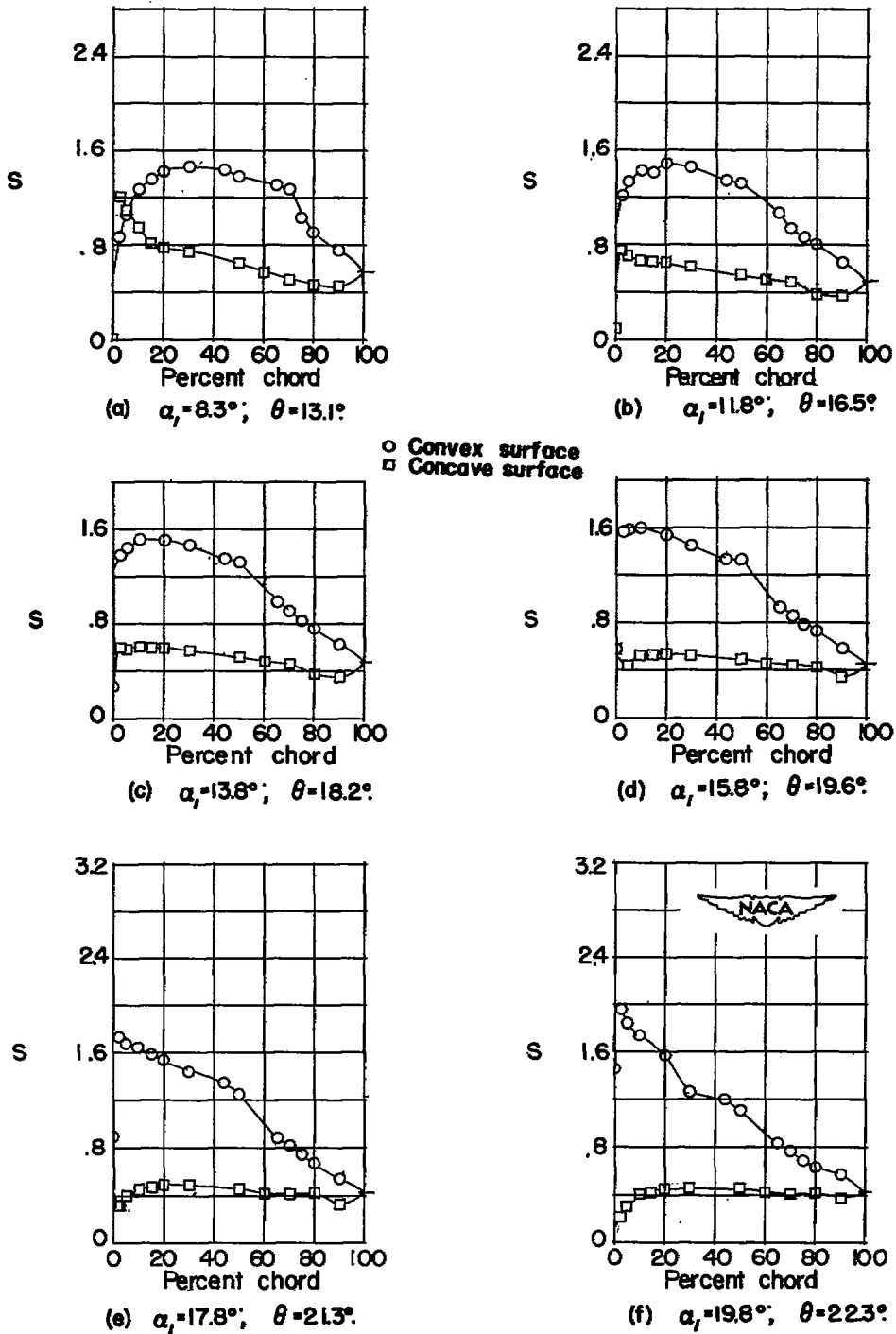
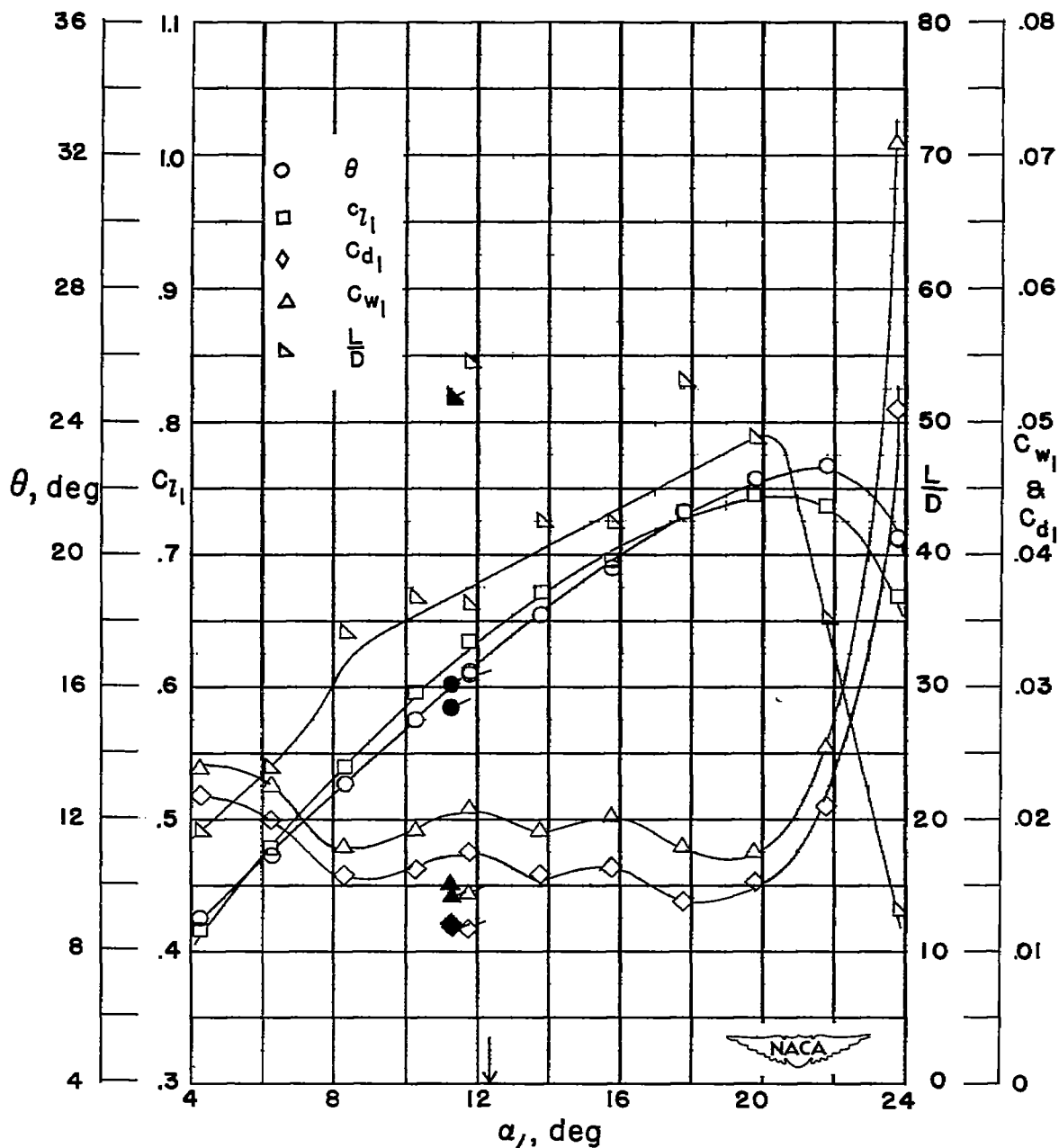


Figure 13.- Blade-surface pressure distributions and blade section characteristics for the cascade combination, $\beta_1 = 60^\circ$, $\sigma = 1.00$, and blade section, 65-(12)12.



(g) Section characteristics; arrow shows design angle of attack, flagged symbol indicates leading-edge roughness; solid symbol indicates high Reynolds number.

Figure 13.- Concluded.

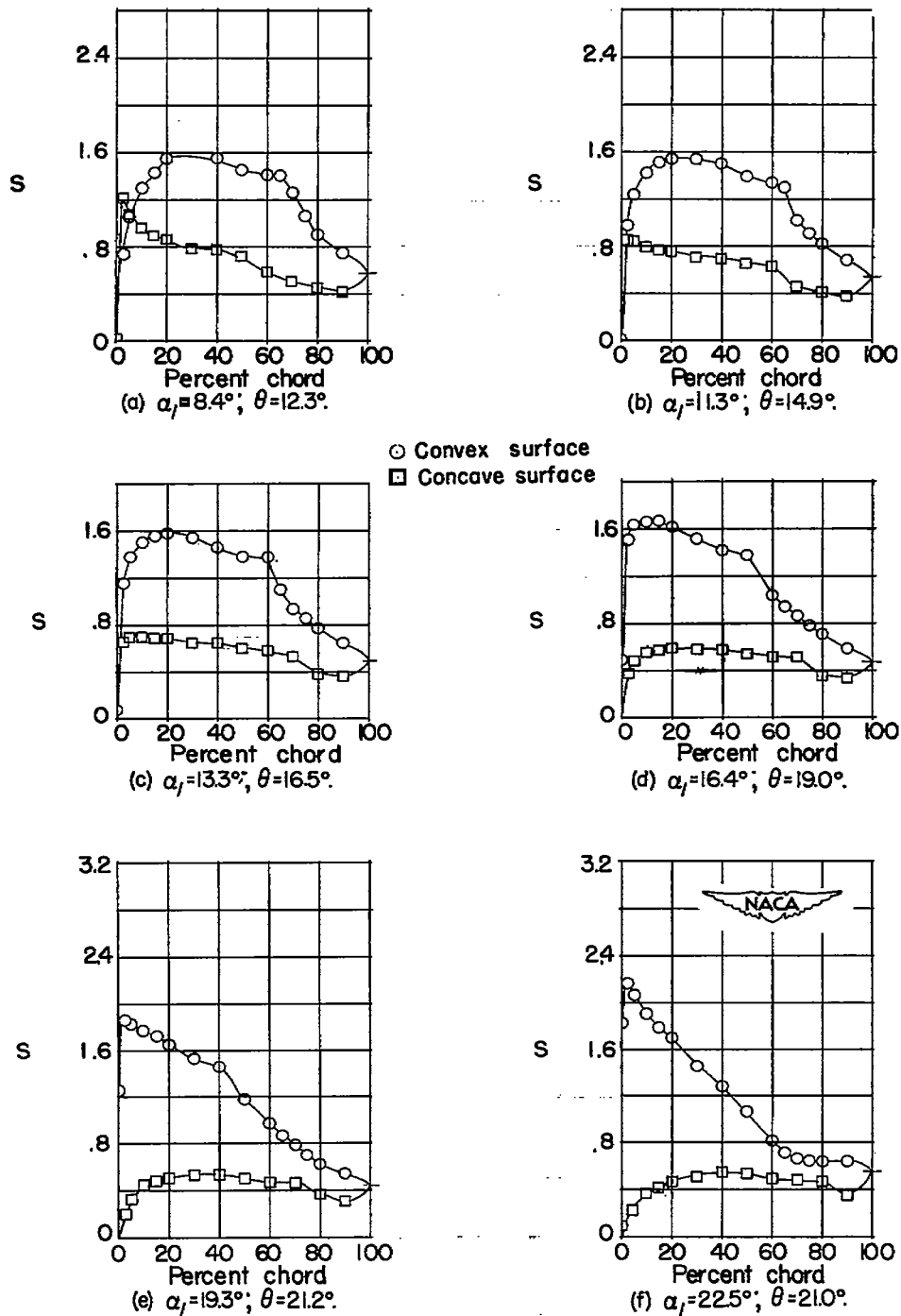
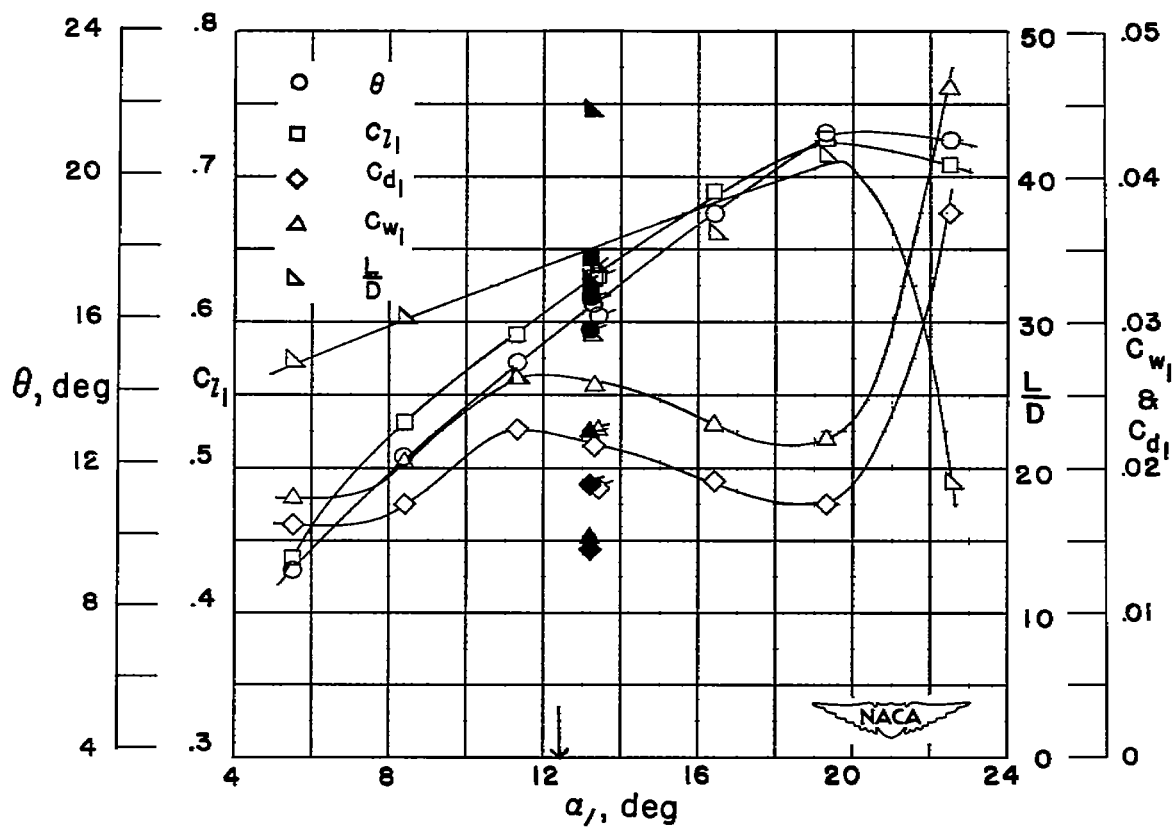


Figure 14.- Blade-surface pressure distributions and blade section characteristics for the cascade combination, $\beta_1 = 60^\circ$, $\sigma = 1.00$, and blade section, 65-(12)15.



(g) Section characteristics; arrow shows design angle of attack, flagged symbol indicates leading-edge roughness; solid symbol indicates high Reynolds number.

Figure 14.- Concluded.

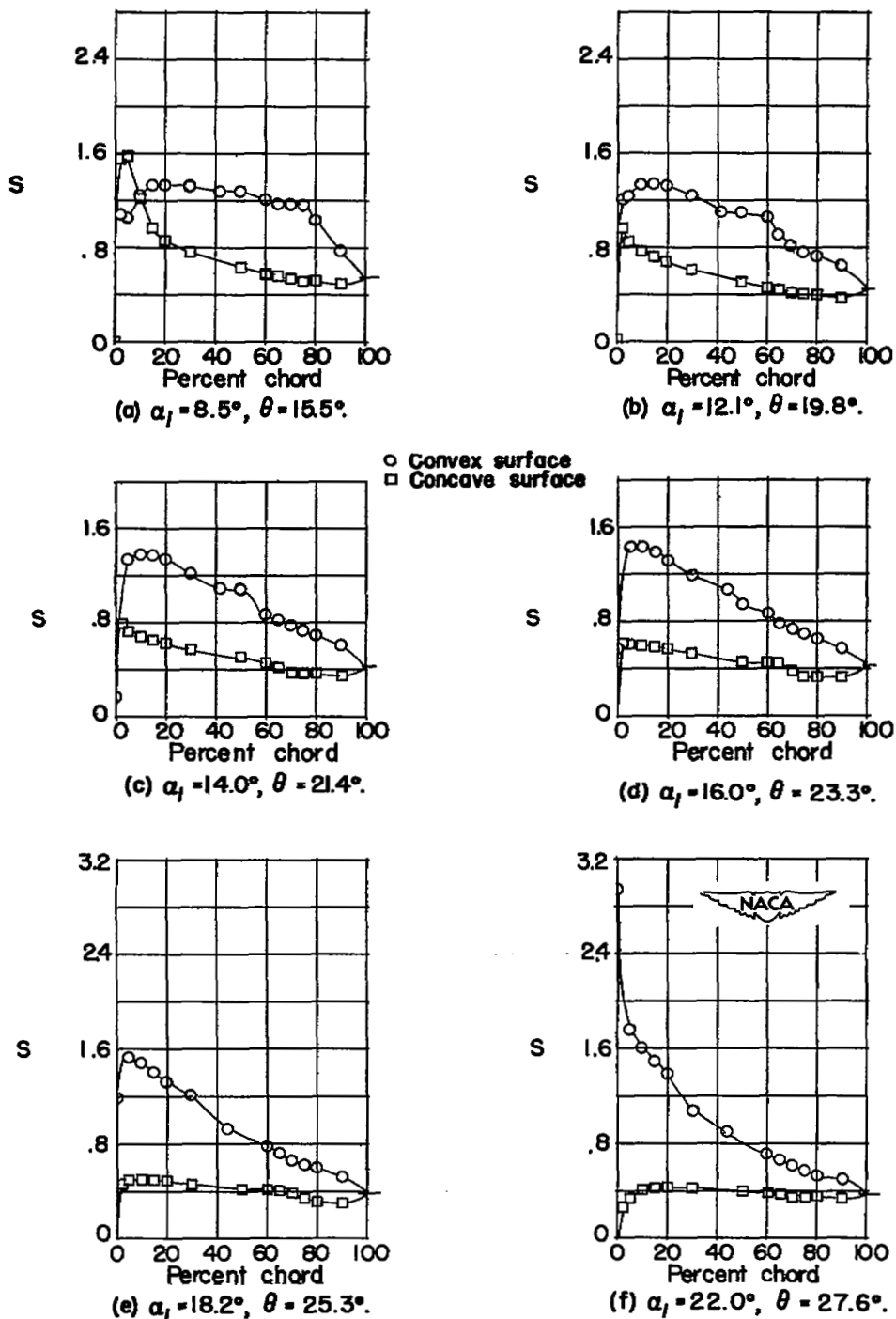
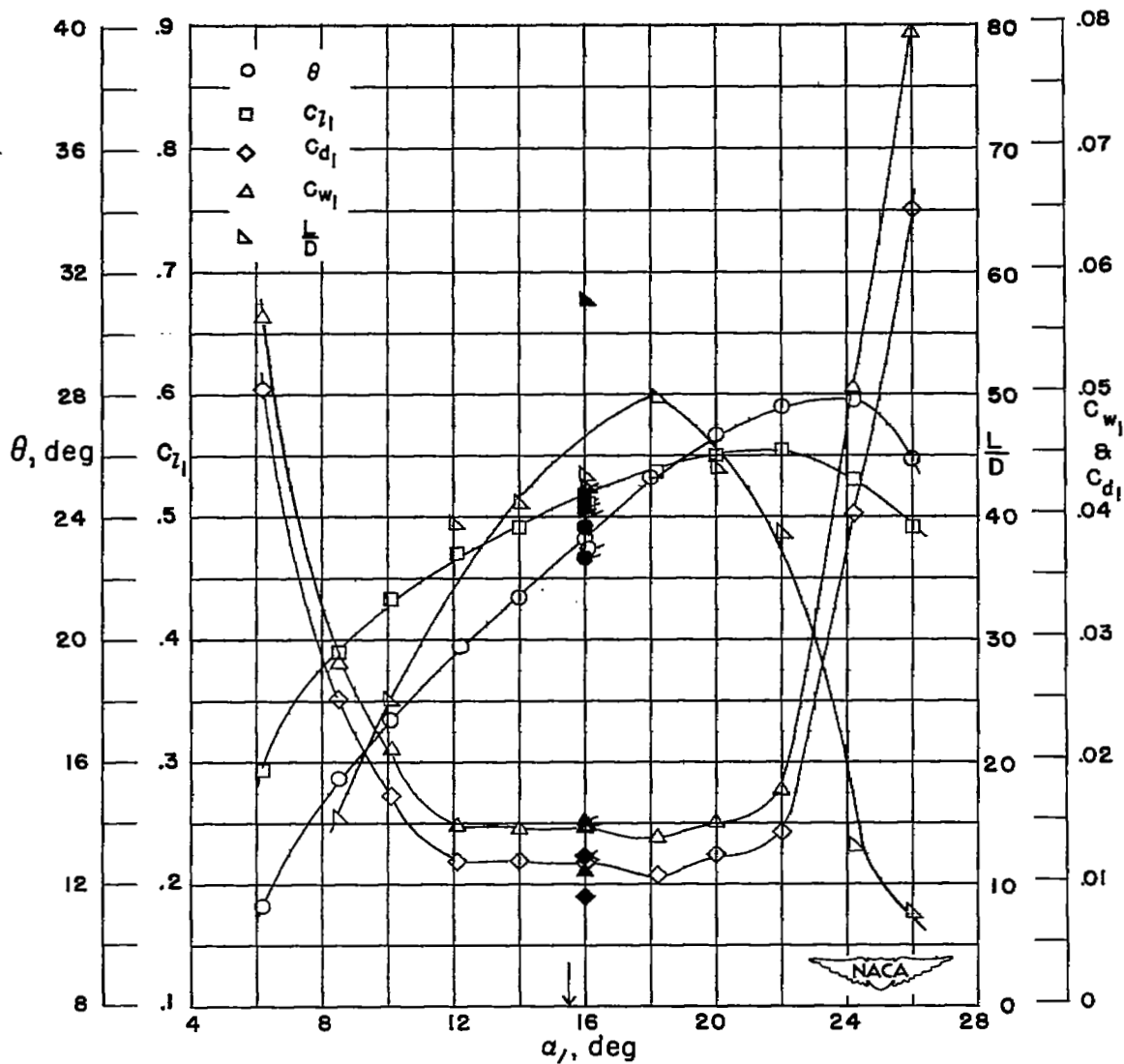


Figure 15.- Blade-surface pressure distributions and blade section characteristics for the cascade combination, $\beta_1 = 60^\circ$, $\sigma = 1.50$, and blade section, 65-(12)06.



(g) Section characteristics; arrow shows design angle of attack; flagged symbol indicates leading-edge roughness; solid symbol indicates high Reynolds number.

Figure 15.- Concluded.

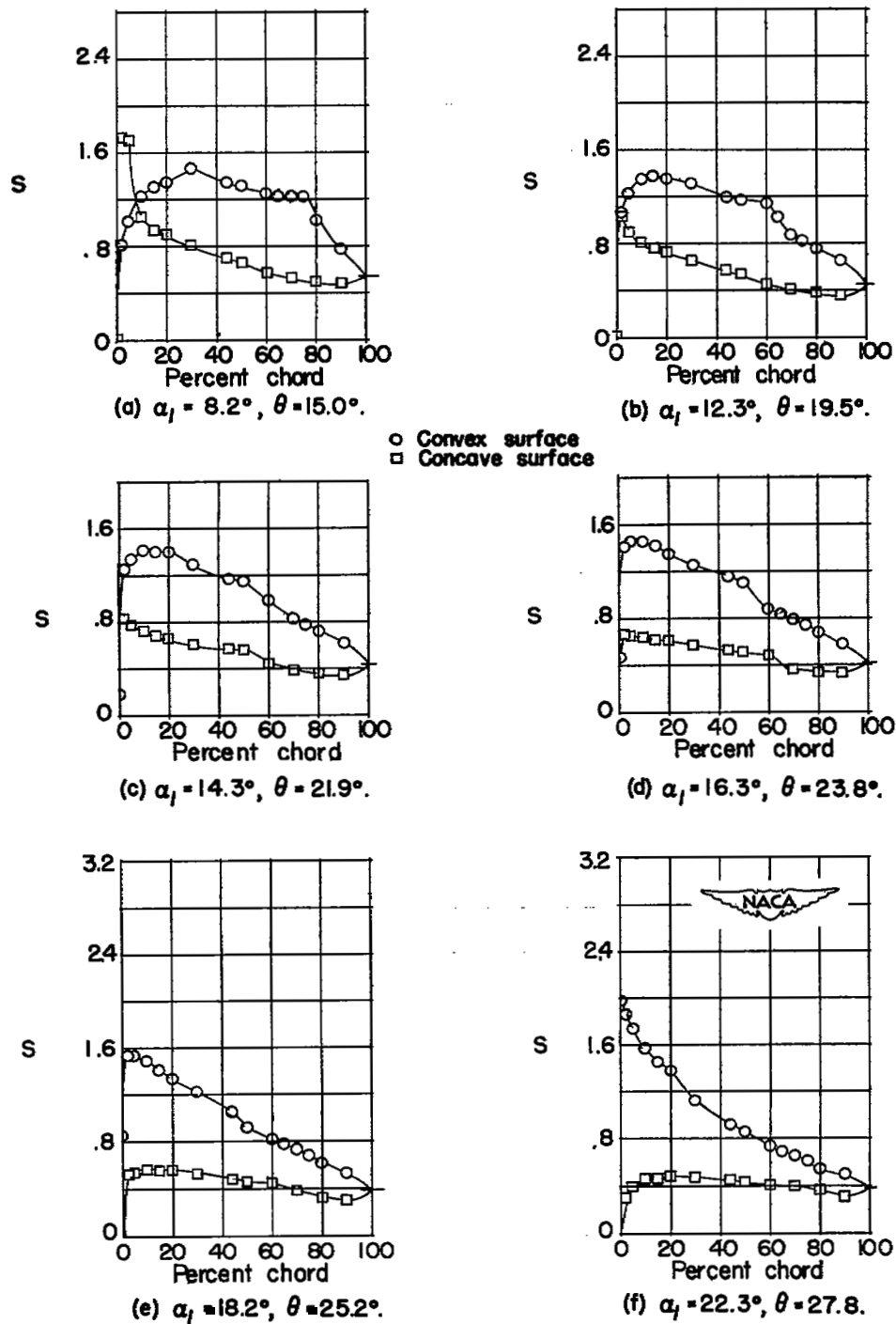
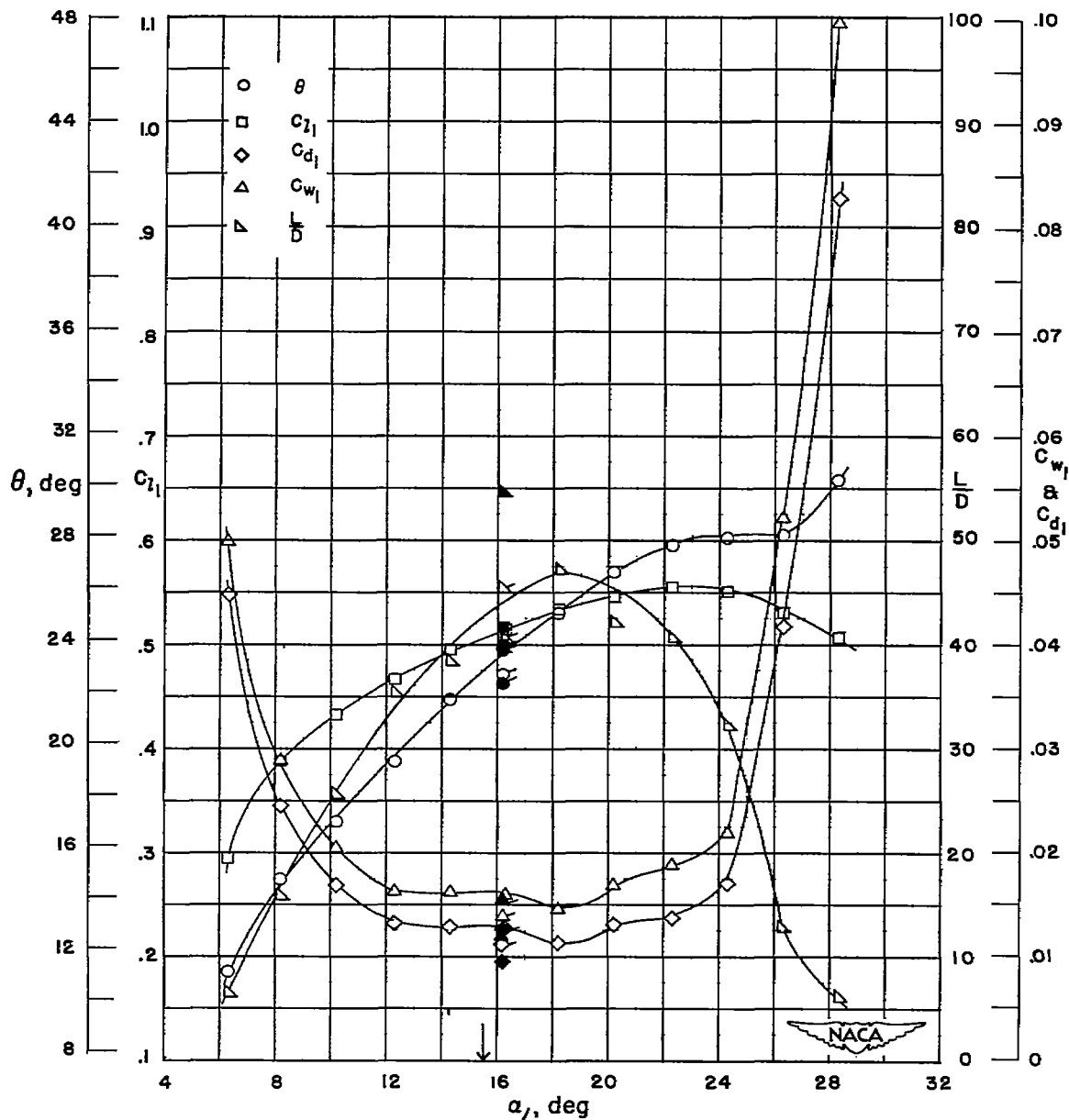


Figure 16.- Blade-surface pressure distributions and blade section characteristics for the cascade combination, $\beta_1 = 60^\circ$, $\sigma = 1.50$, and blade section, 65-(12)08.



(g) Section characteristics; arrow shows design angle of attack; flagged symbol indicates leading-edge roughness; solid symbol indicates high Reynolds number.

Figure 16.- Concluded.

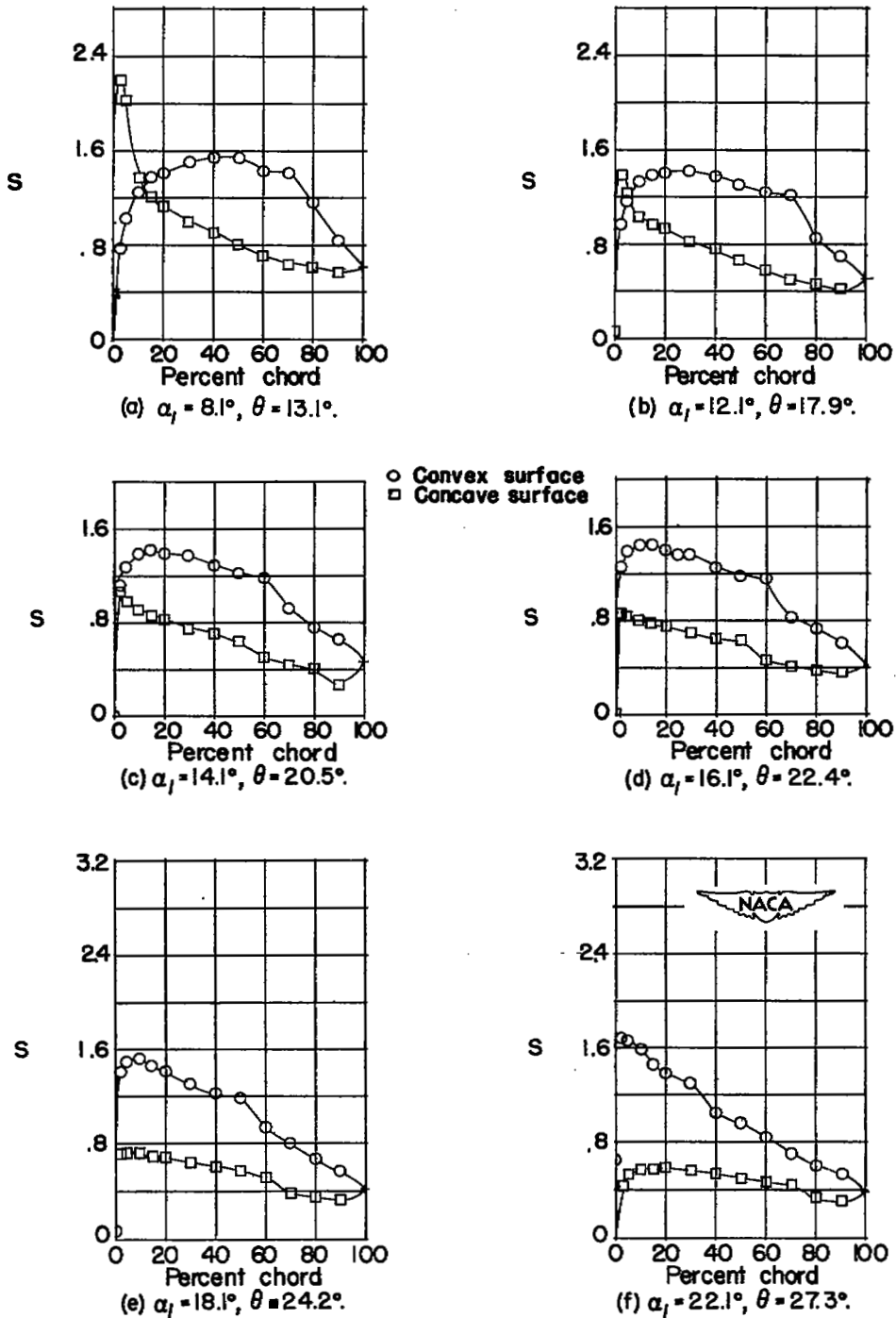
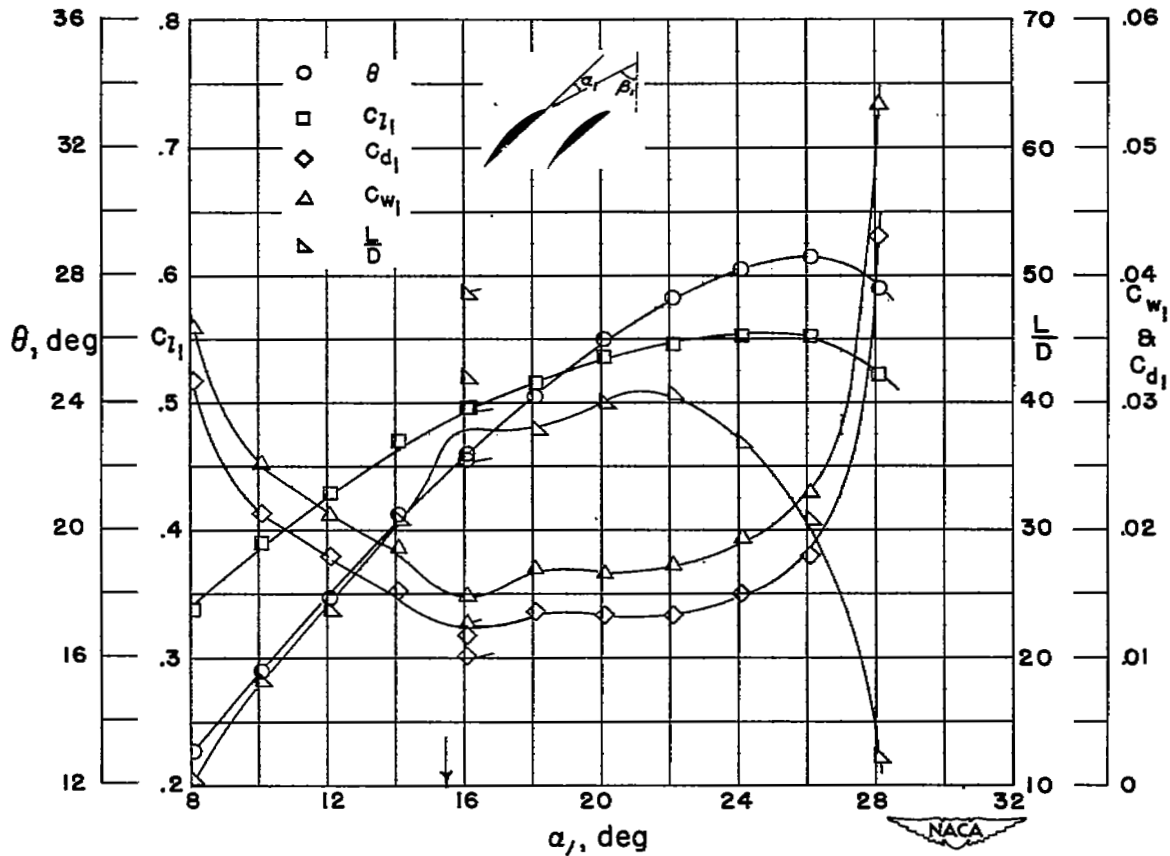


Figure 17.- Blade-surface pressure distributions and blade section characteristics for the cascade combination, $\beta_1 = 60^\circ$, $\sigma = 1.50$, and blade section, 65-(12)10.

7F



(g) Section characteristics, arrow shows design angle of attack; flagged symbol indicates leading-edge roughness

Figure 17.- Concluded.

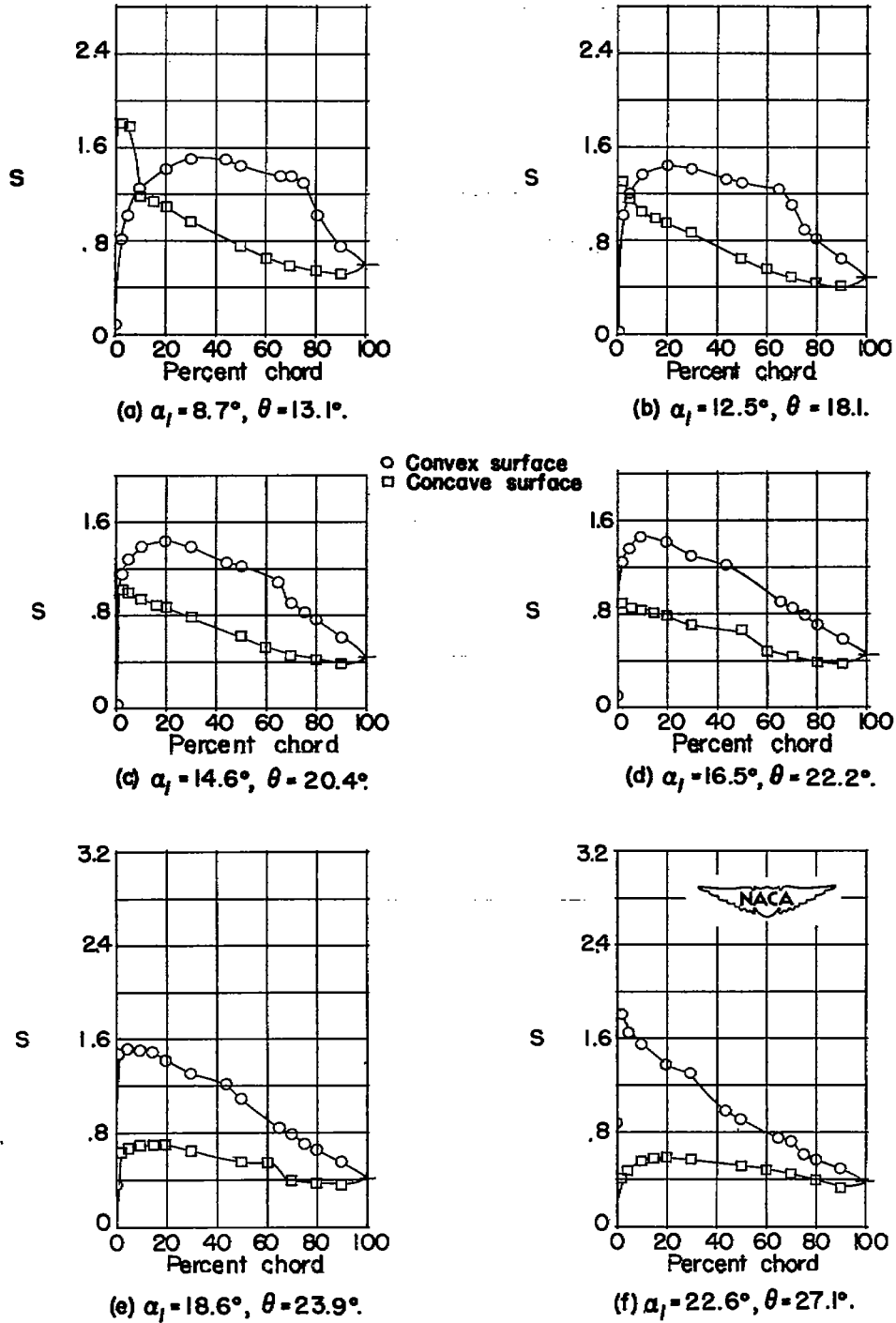
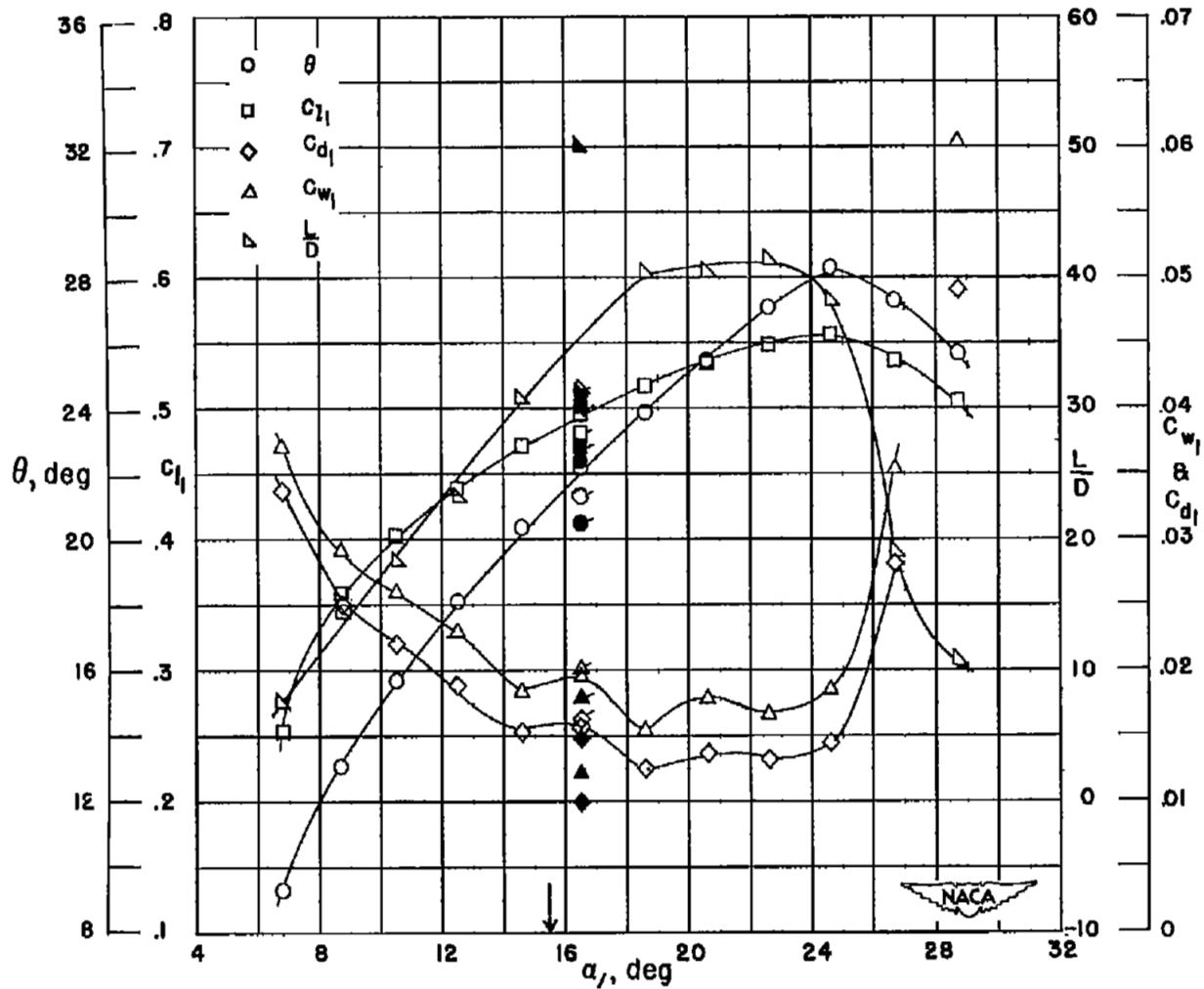


Figure 18.- Blade-surface pressure distributions and blade section characteristics for the cascade combination, $\beta_1 = 60^\circ$, $\sigma = 1.50$, and blade section, 65-(12)12.



(g) Section characteristics; arrow shows design angle of attack; flagged symbol indicates leading-edge roughness; solid symbol indicates high Reynolds number.

Figure 18.- Concluded.

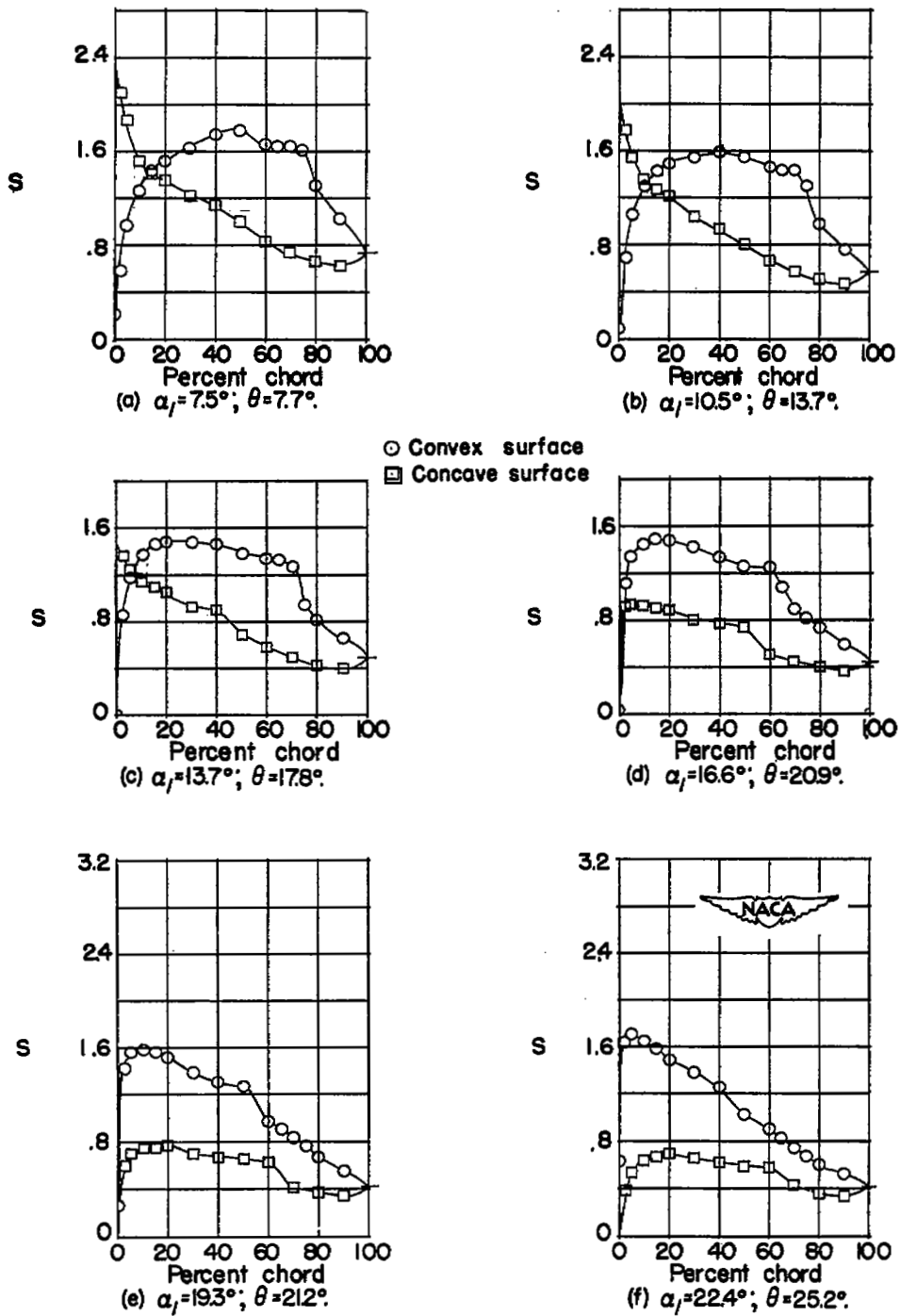
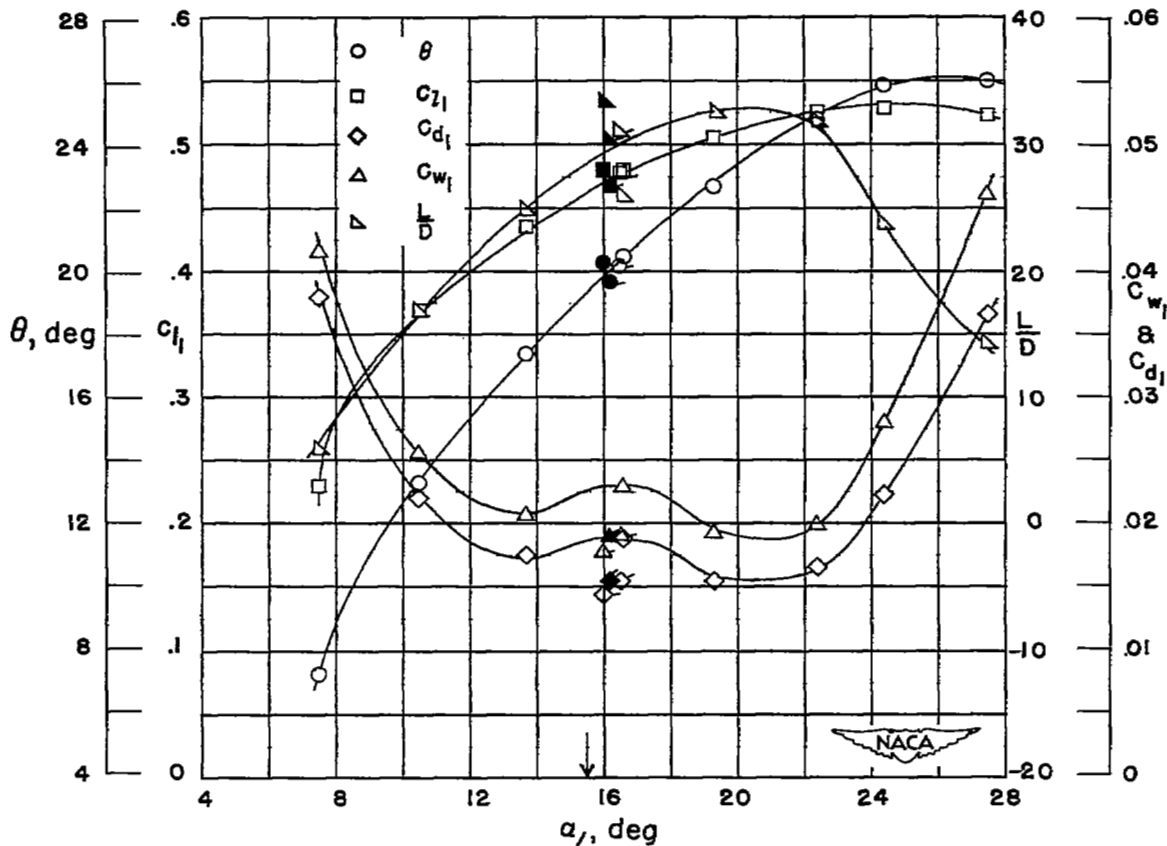
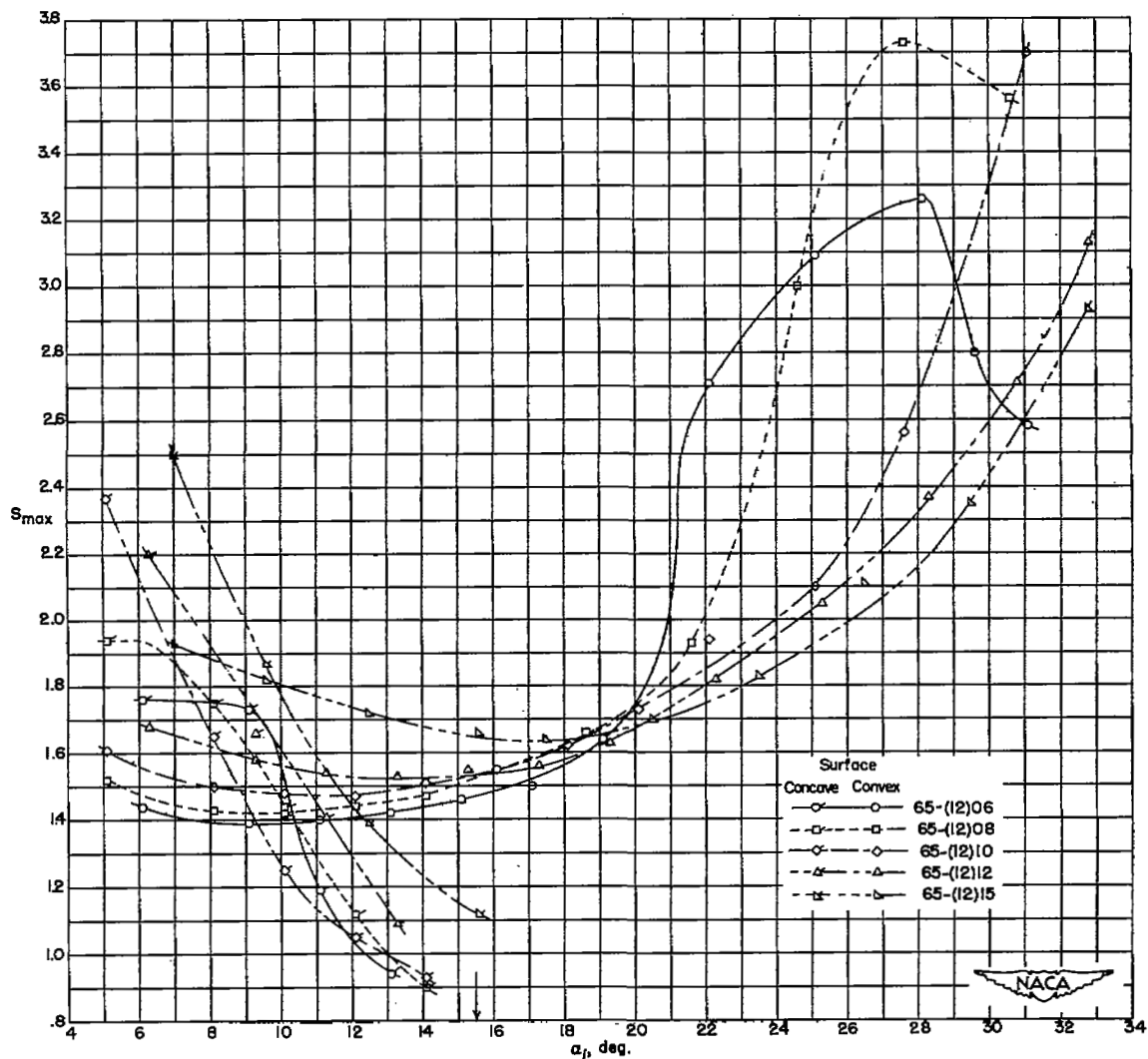


Figure 19.- Blade-surface pressure distributions and blade section characteristics for the cascade combination, $\beta_1 = 60^\circ$, $\sigma = 1.50$, and blade section, 65-(12)15.



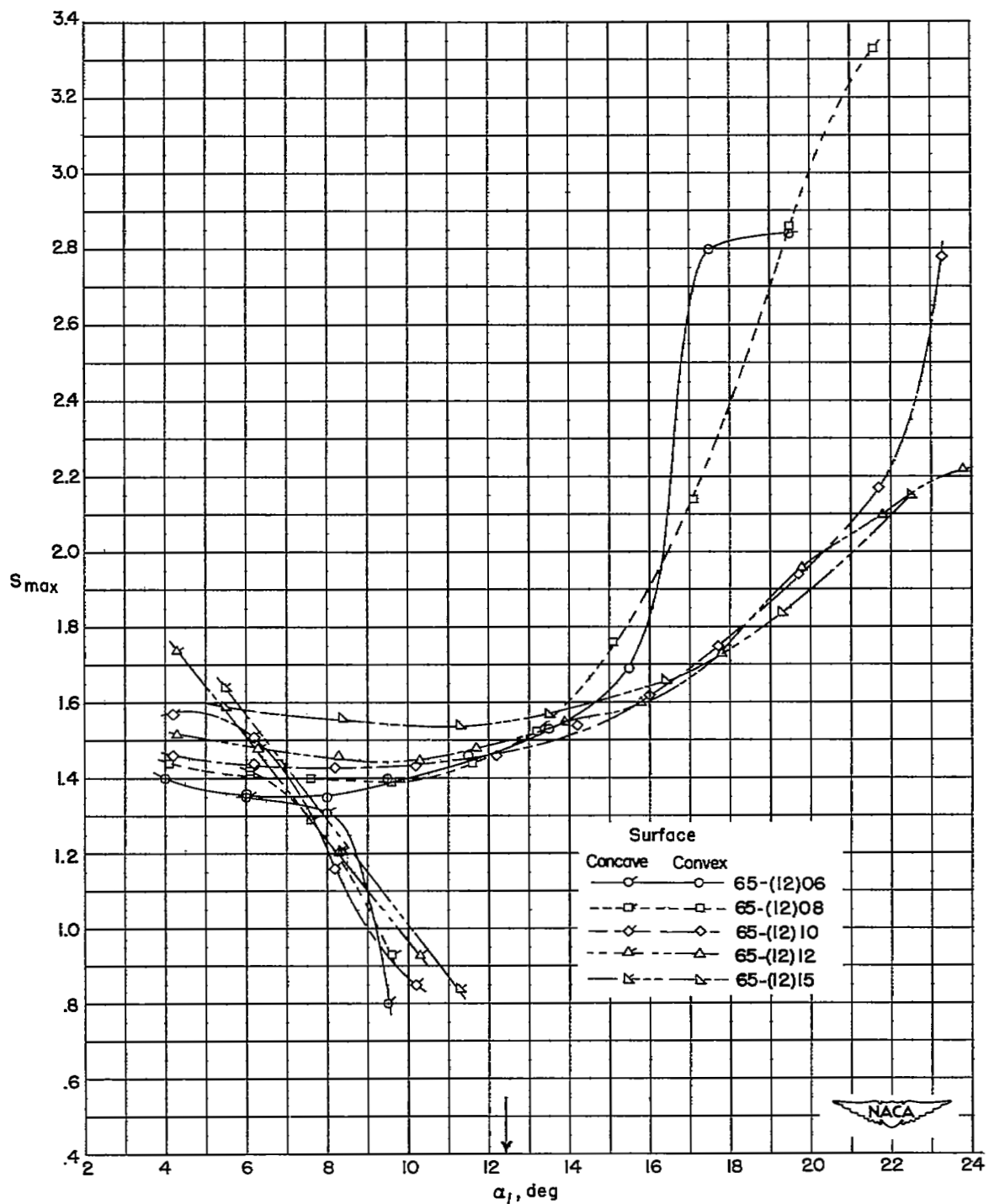
(g) Section characteristics; arrow shows design angle of attack; flagged symbol indicates leading-edge roughness; solid symbol indicates high Reynolds number.

Figure 19.- Concluded.



(a) $\beta = 45^\circ$, $\sigma = 1.5$.

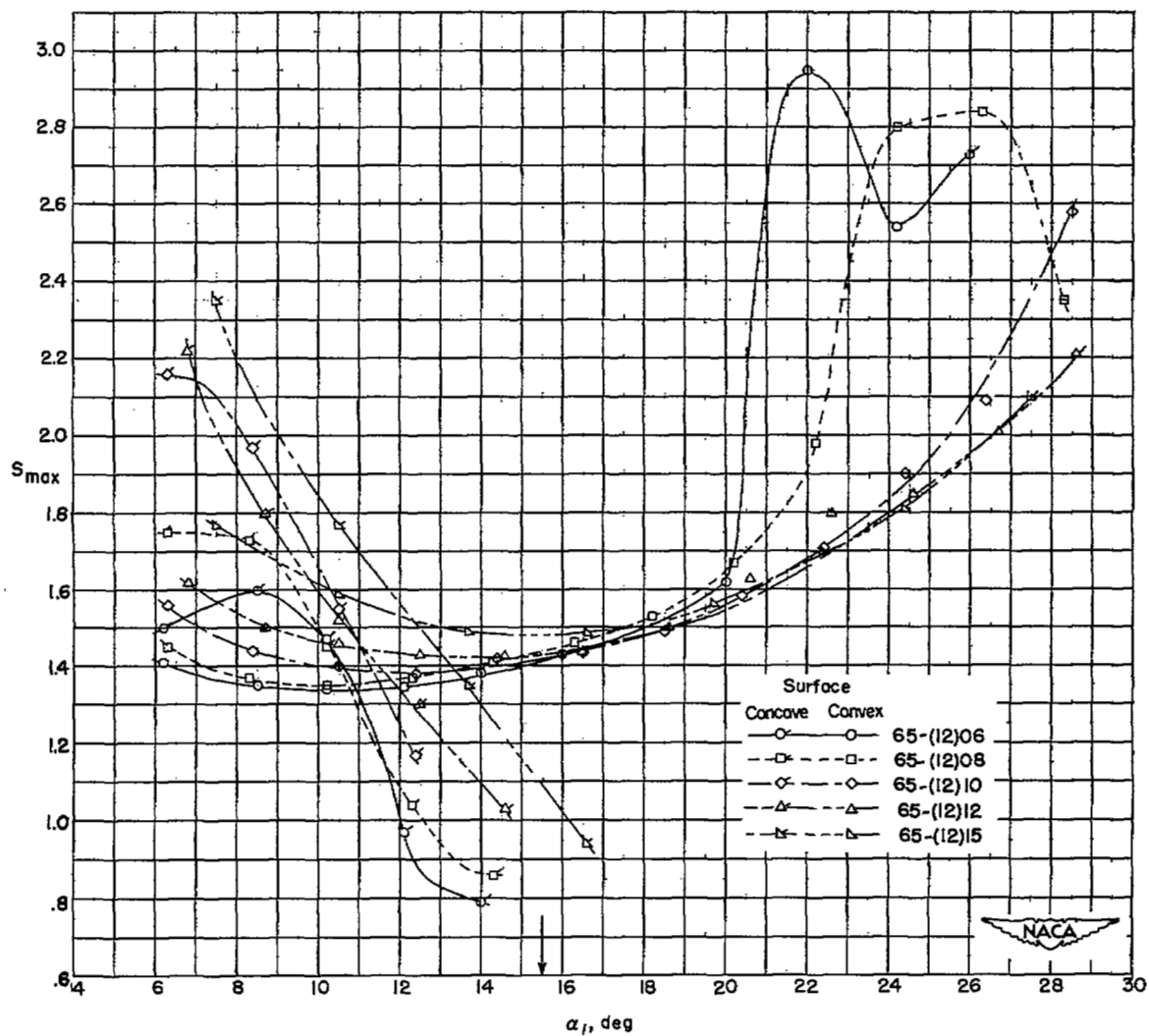
Figure 20.- Variation of maximum pressure coefficient on upper and lower blade surfaces with angle of attack for sections of varying thickness.



(b) $\beta = 60^\circ$, $\sigma = 1.0$.

Figure 20.- Continued.

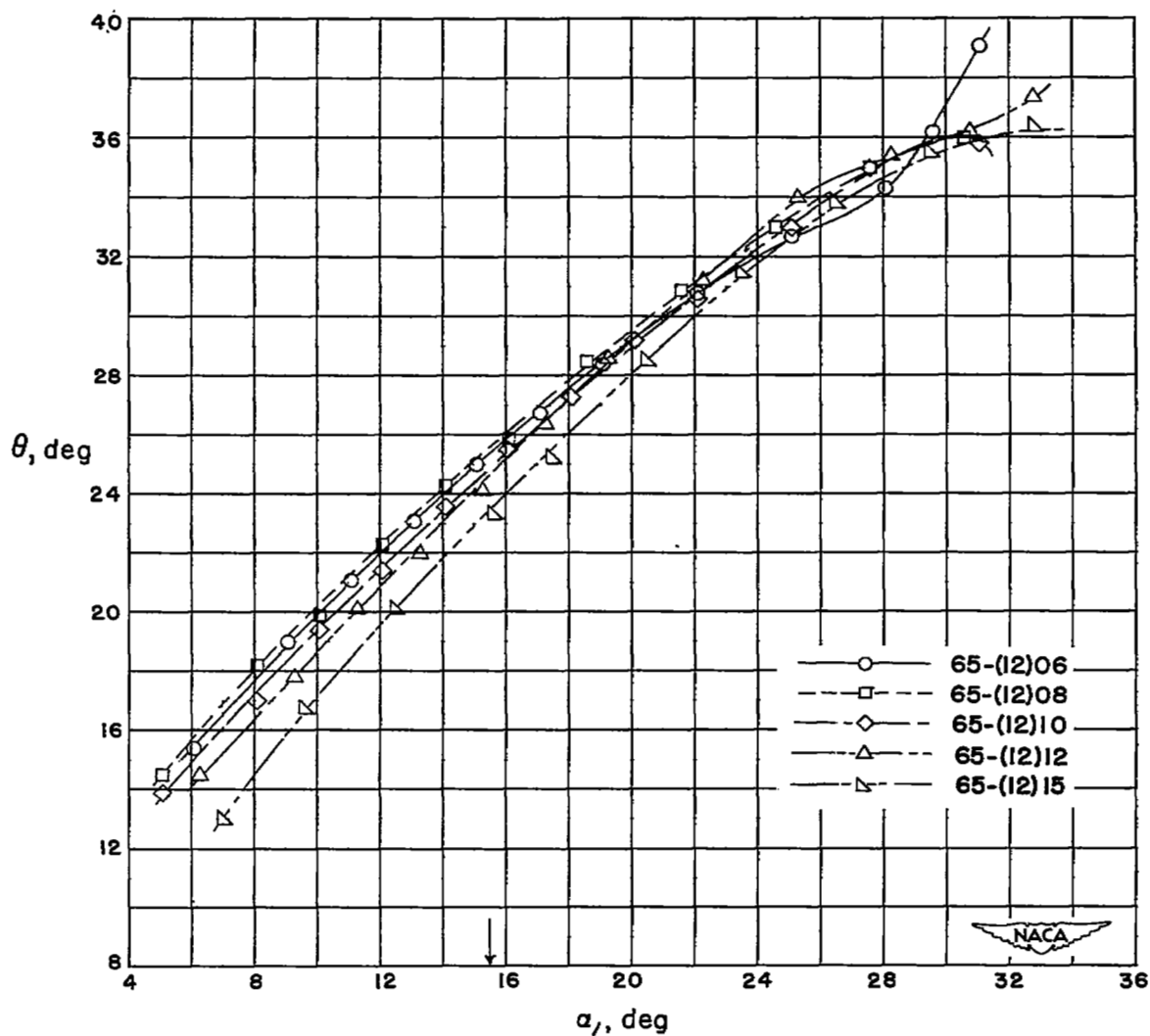
~~CONFIDENTIAL~~

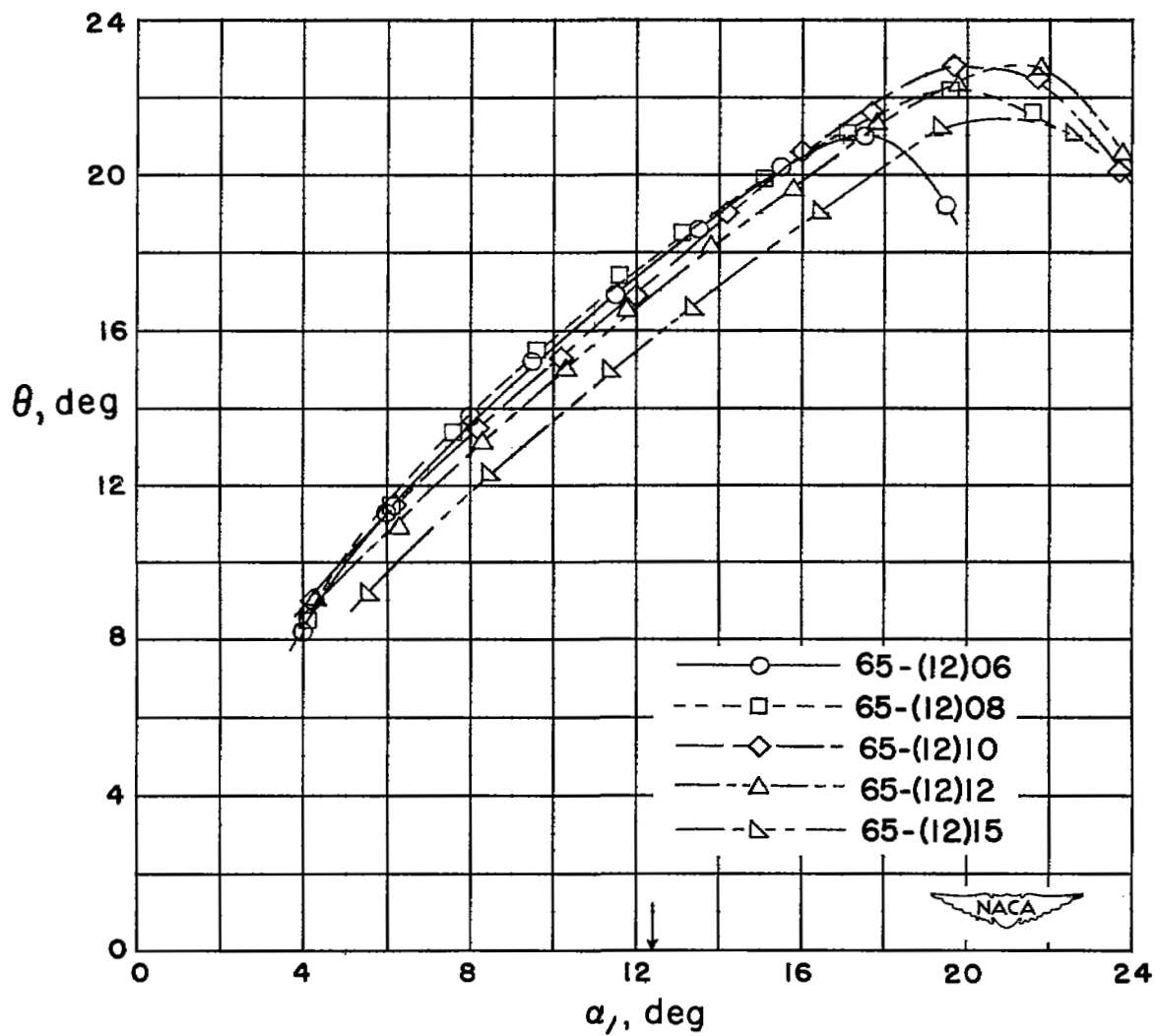


(c) $\beta = 60^\circ$, $\sigma = 1.5$.

Figure 20.- Concluded.

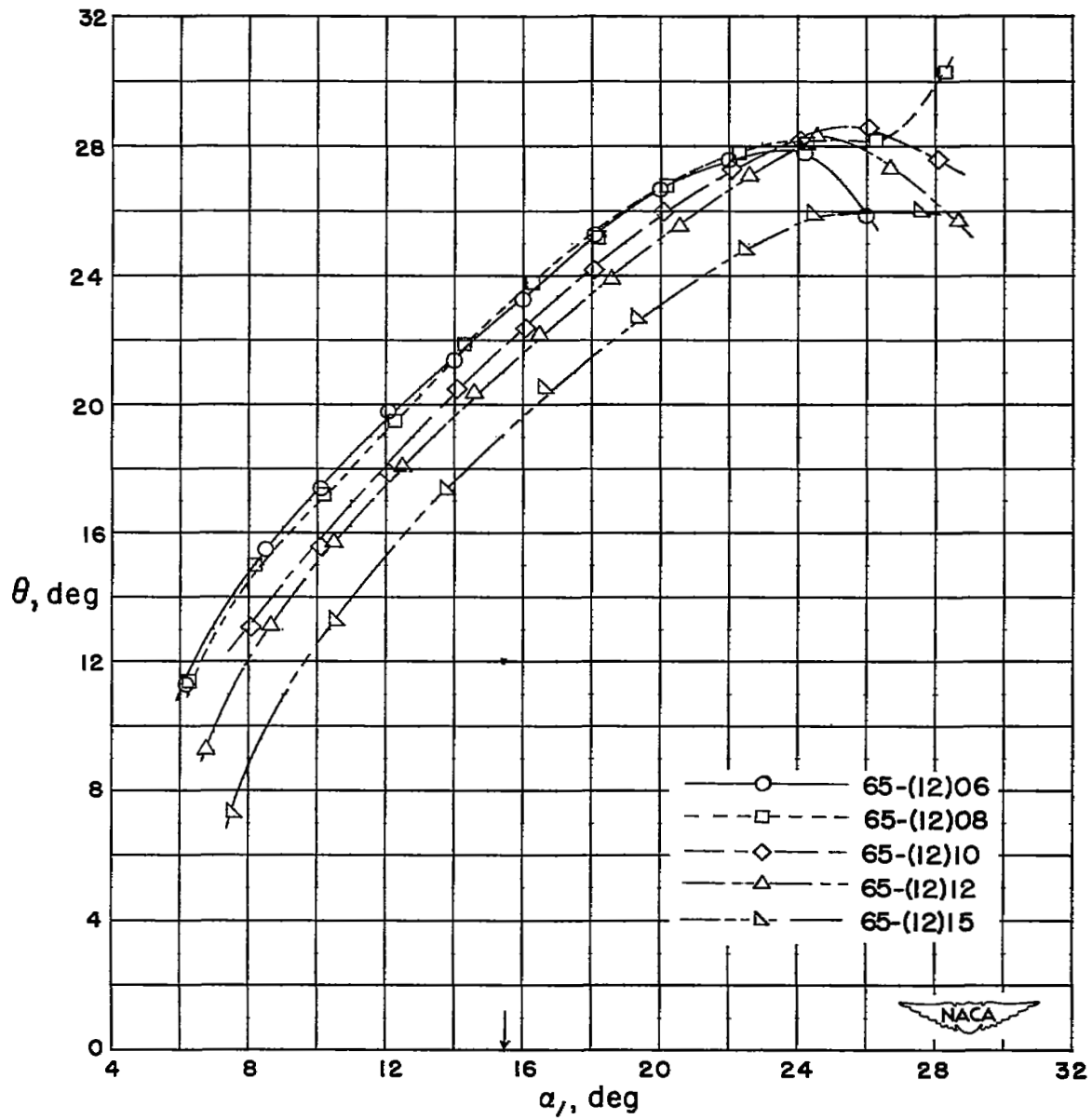
8F

(a) $\beta_1 = 45^\circ$, $\sigma = 1.5$.Figure 21.- Summary of turning angle, θ , angle of attack, α , relationship for the blade sections tested.



(b) $\beta_1 = 60^\circ$, $\sigma = 1.0$.

Figure 21.- Continued.



(c) $\beta_1 = 60^\circ$, $\sigma = 1.5$.

Figure 21.- Concluded.

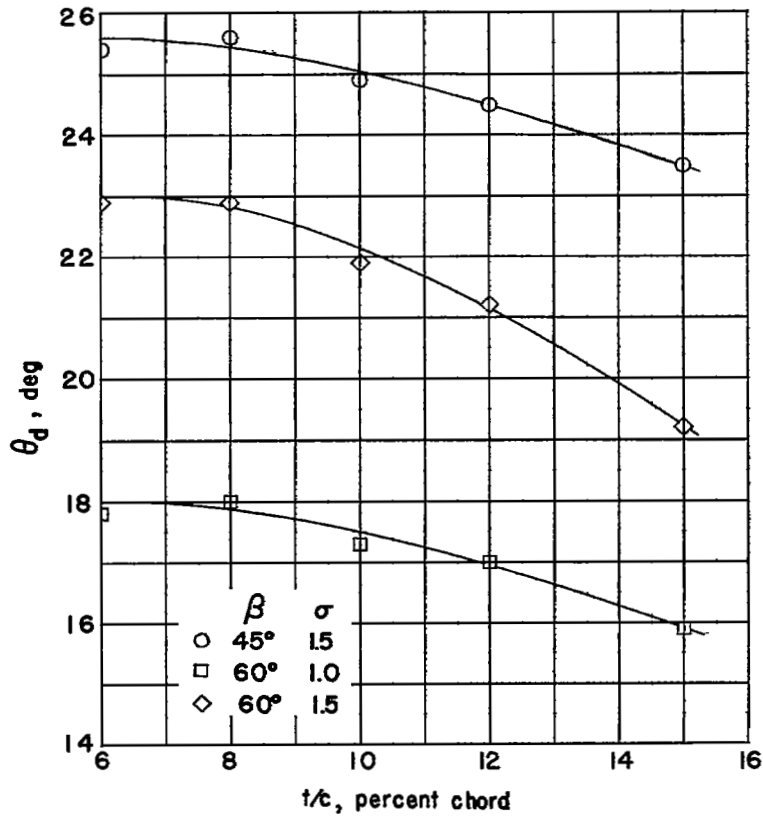
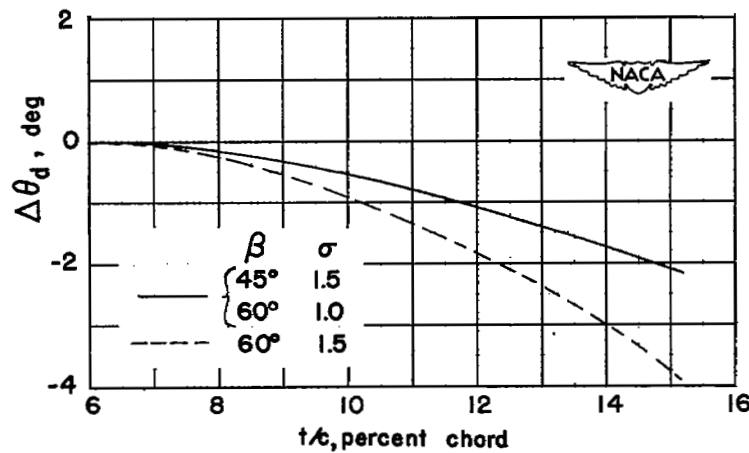
(a) Variation of design turning angle, θ_d , deg.(b) Design turning angle change, $\Delta\theta_d$, deg.

Figure 22.- Effect of change in maximum thickness ratio t/c on the design turning angle of the 65-(12) t/c blade section for several combinations of inlet angle and solidity.

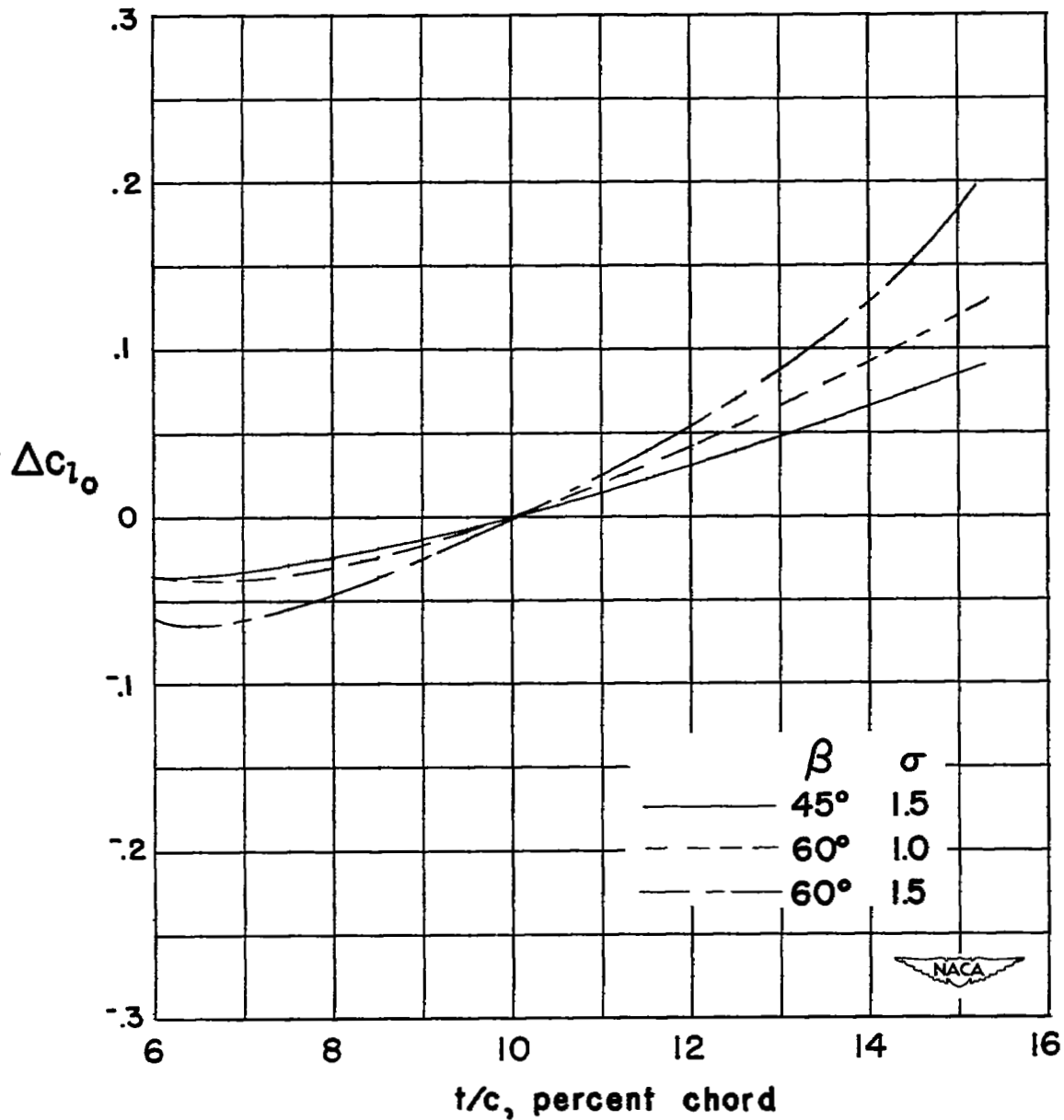


Figure 23.- Variation of camber change Δc_{l_0} with maximum thickness ratio t/c required to maintain the design turning angle of the 65-(12)10 blade section.

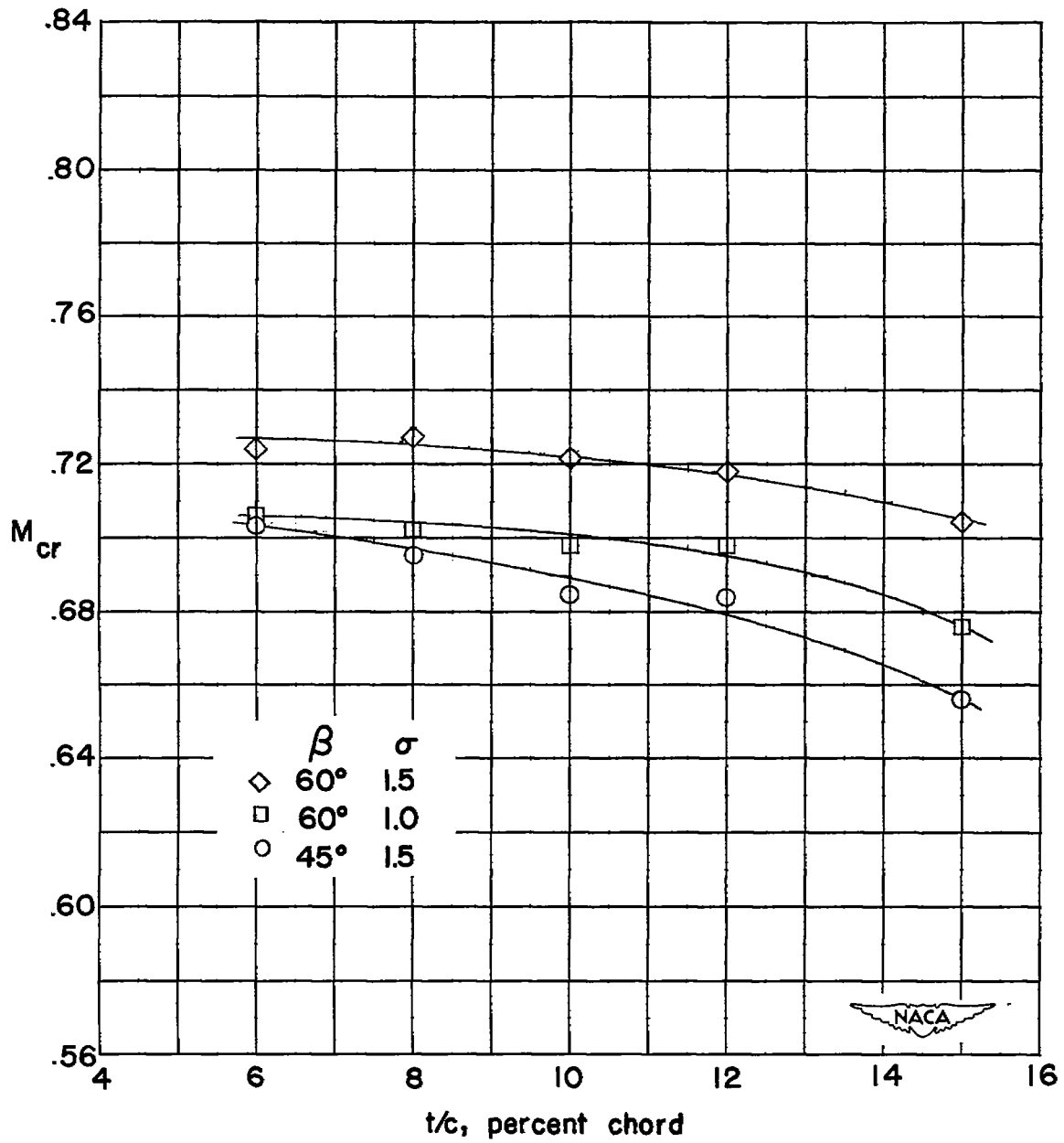
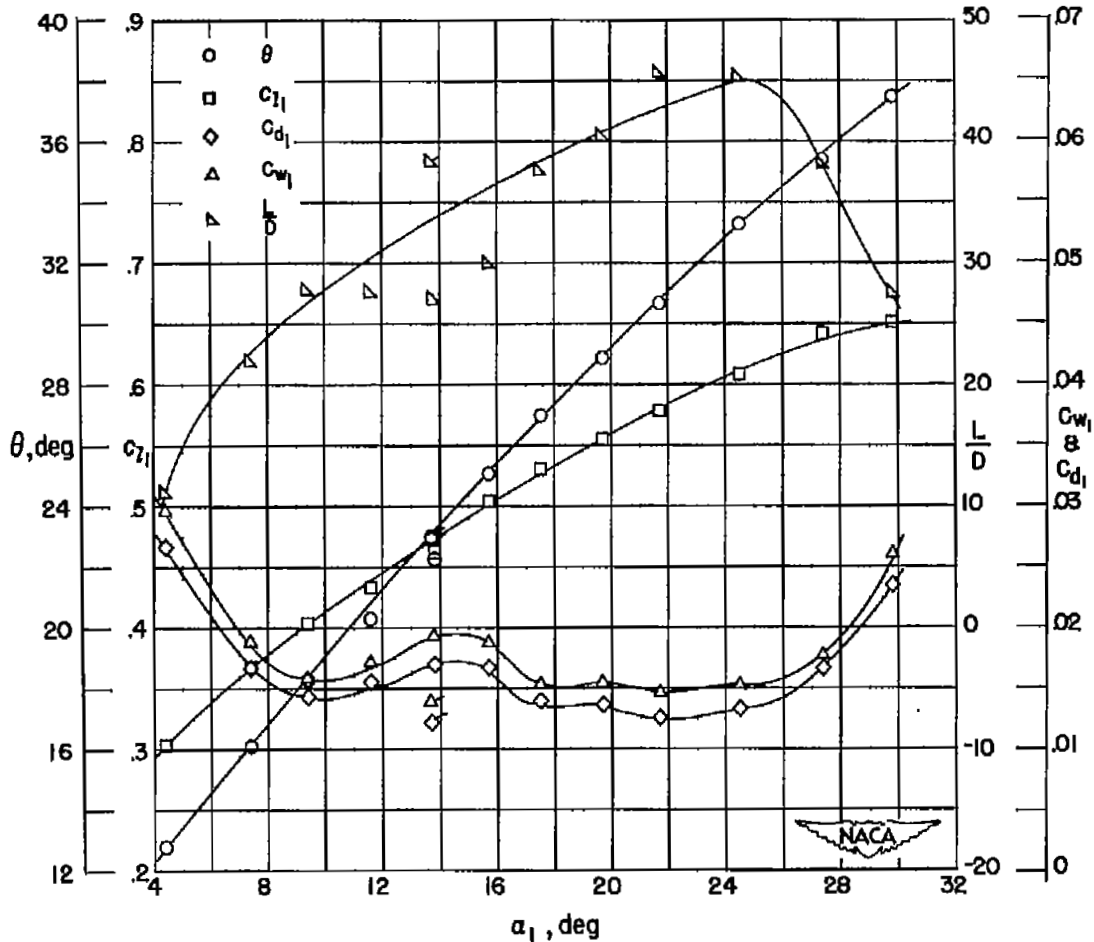
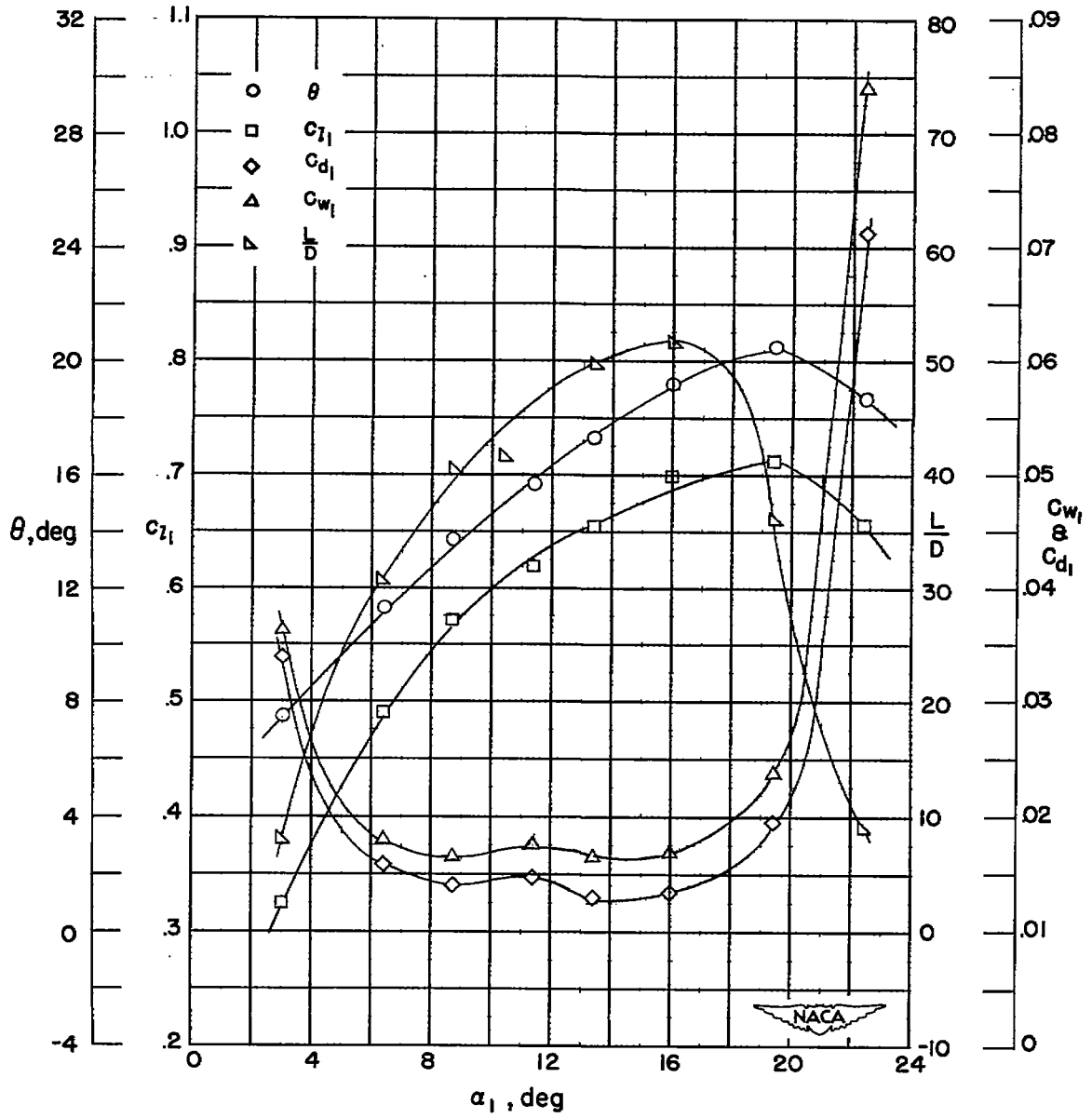


Figure 24.- Variation of estimated critical Mach number M_{cr} with section thickness at design angles of attack.



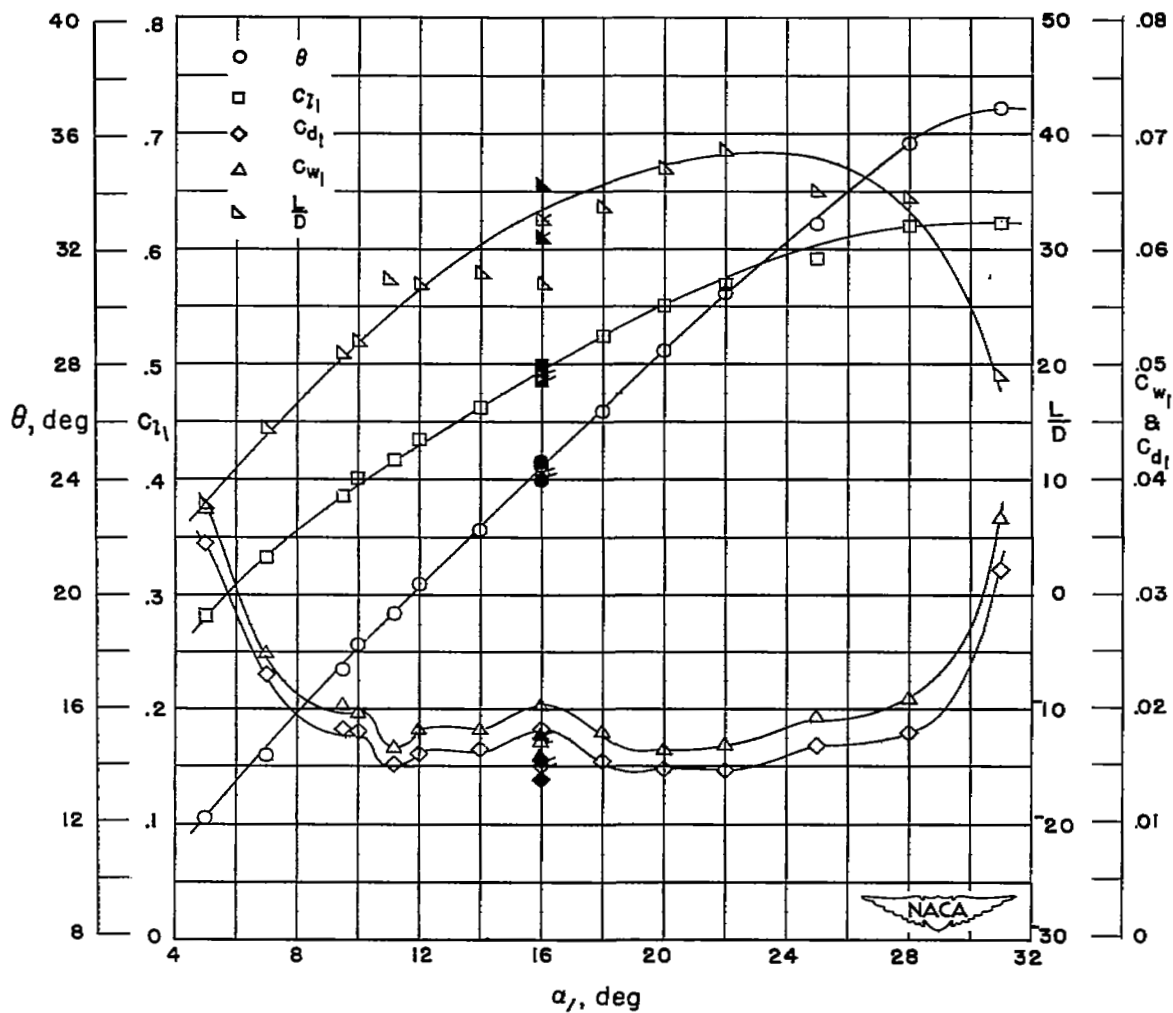
(a) $\beta = 45^\circ, \sigma = 1.5.$

Figure 25.- Section operating characteristics of the NACA 65-(12)10 compressor blade having a 1-percent-chord trailing-edge radius.



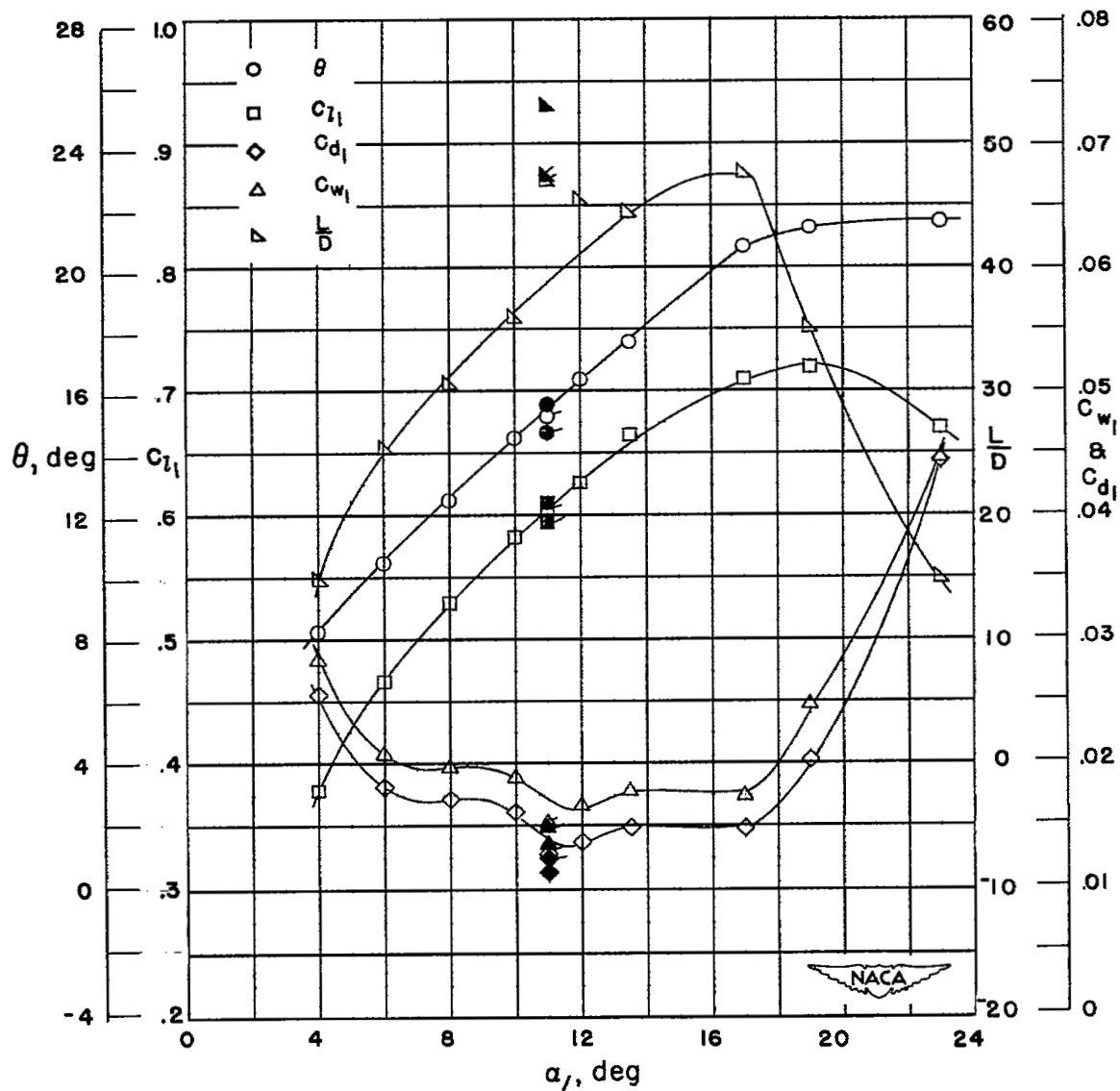
(b) $\beta = 60^\circ$, $\sigma = 1.0$.

Figure 25.- Concluded.



(a) $\beta = 45^\circ$, $\sigma = 1.5$.

Figure 26.- Section operating characteristics of the NACA 65-(12)10 compressor blade having a 2-percent-chord trailing-edge radius.



(b) $\beta = 60^\circ$, $\sigma = 1.0$.

Figure 26.- Concluded.

NASA Technical Library



3 1176 01436 8881

4
3
14

